Spanning the scales of mechanical metamaterials using time domain simulations in transformed crystals, graphene flakes and structured soils

Ronald Aznavourian, Tania M Puvirajesinghe, Stéphane Brulé, Stefan Enoch, Sébastien Guenneau

OPEN ACCESS
IOP Publishing
Journal of Physics: Condensed Matter
J. Phys.: Condens. Matter **29** (2017) 433004 (20pp)
https://doi.org/10.1088/1361-648X/aa81ff

Topical Review

Spanning the scales of mechanical metamaterials using time domain simulations in transformed crystals, graphene flakes and structured soils

Ronald Aznavourian[1], Tania M Puvirajesinghe[2,3], Stéphane Brûlé[4], Stefan Enoch[1] and Sébastien Guenneau[1,5]

[1] CNRS, Centrale Marseille, Institut Fresnel UMR 7249, Aix-Marseille Université, 13013 Marseille, France
[2] CRCM, Cell Polarity, Cell signaling and Cancer, "Equipe Labellisée Ligue Contre le Cancer", Inserm, U1068, Aix-Marseille Université, Marseille, F-13009, France
[3] Institut Paoli-Calmettes, Marseille, F-13009, France
[4] Dynamic Soil Laboratory, Ménard, 91620 Nozay, France

E-mail: sebastien.guenneau@fresnel.fr and tania.guenneau-puvirajesinghe@inserm.fr

Received 10 April 2016, revised 24 July 2017
Accepted for publication 25 July 2017
Published 27 September 2017

Abstract

We begin with a brief historical survey of discoveries of quasi-crystals and graphene, and then introduce the concept of transformation crystallography, which consists of the application of geometric transforms to periodic structures. We consider motifs with three-fold, four-fold and six-fold symmetries according to the crystallographic restriction theorem. Furthermore, we define motifs with five-fold symmetry such as quasi-crystals generated by a cut-and-projection method from periodic structures in higher-dimensional space. We analyze elastic wave propagation in the transformed crystals and (Penrose-type) quasi-crystals with the finite difference time domain freeware SimSonic. We consider geometric transforms underpinning the design of seismic cloaks with square, circular, elliptical and peanut shapes in the context of honeycomb crystals that can be viewed as scaled-up versions of graphene. Interestingly, the use of morphing techniques leads to the design of cloaks with interpolated geometries reminiscent of Victor Vasarely's artwork. Employing the case of transformed graphene-like (honeycomb) structures allows one to draw useful analogies between large-scale seismic metamaterials such as soils structured with columns of concrete or grout with soil and nanoscale biochemical metamaterials. We further identify similarities in designs of cloaks for elastodynamic and hydrodynamic waves and cloaks for diffusion (heat or mass) processes, as these are underpinned by geometric transforms. Experimental data extracted from field test analysis of soil structured with boreholes demonstrates the application of crystallography to large scale phononic crystals, coined as seismic metamaterials, as they might exhibit low frequency stop bands. This brings us to the outlook of mechanical metamaterials, with control

[5] Author to whom any correspondence should be addressed.

of phonon emission in graphene through extreme anisotropy, attenuation of vibrations of suspension bridges via low frequency stop bands and the concept of transformed meta-cities. We conclude that these novel materials hold strong applications spanning different disciplines or across different scales from biophysics to geophysics.

Keywords: computational methods, time domain simulations, geometric transforms, metamaterials, invisibility cloaks, morphing, geophysics

S Supplementary material for this article is available online

(Some figures may appear in colour only in the online journal)

1. Introduction

In 2011, the Israeli physicist Dan Shechtman received the Nobel Prize in chemistry for his discovery of a phase of an aluminum-manganese alloy (Al with 10–14 percent of Mn, Fe or Cr) with a five-fold symmetry originally carried out in 1984. In this breakthrough article [1] Shechtman together with his colleagues Ilian Blech (an Israeli physicist), John Werner Cahn (an American scientist) and Denis Gratias (a French mathematical crystallographer) discovered that this crystalline-like substance goes beyond the crystallographic restriction theorem, which states that the only rotational symmetries allowed for a crystalline pattern (i.e. a discrete system of points with a translational symmetry) display two-fold, three-fold, four-fold and six-fold symmetries. Five-fold rotational symmetry, as well as any other symmetry beyond six-fold, is forbidden in periodic structures, and was thought to not exist in nature, until the discovery of the icosahedrite ($Al_{63}Cu_{24}Fe_{13}$), which is a mineral found by an international team led by Luca Bindi (an Italian geologist) and Paul Steinhardt (an American cosmologist). One year previous to Shechtman's Nobel Prize, the Dutch-British physicist Sir Andrei Konstantinovich Geim and his Russian-British colleague Sir Konstantin Sergeevich Novolesov received the Nobel Prize in physics for their discovery of graphene in 2004 [2]. Graphene is a one-atom thick layer of graphite (a crystalline form of carbon) with six-fold symmetry. A top view of graphene reveals a honeycomb lattice as shown in figure 1(a), consisting of one atom of carbon at each vertex of the 6-ring structure. Geim and Novoselov demonstrated the difference between graphene and graphite by using adhesive to isolate graphene (less than one nanometer thick) sheets away from graphite. Achieving single layers of graphene typically requires multiple exfoliation steps. Importantly, the acoustic and thermal properties of graphite, and thus graphene, are extremely anisotropic, since phonons propagate very fast along the tightly-bound planes, but much slower from one plane to another. This opens new vistas in wave physics as anisotropy is actually at the base of metamaterials, which makes possible the control of wave trajectories thanks to resonant subwavelengths elements (typically a few tenths of nanometers in size for visible light), enabling extreme effective tunable anisotropy.

The discoveries of quasi-crystals in 1984 and graphene in 2004 have revolutionized material sciences and given birth to new research areas in chemistry, biosciences, mechanical sciences and optics, amongst many disciplines. Interestingly, graphene flakes, which can be as small as a few tenths of nanometres in size, self-organize like clay in stratified soils, as noted in [3], and allow enhanced control of diffusion processes through effective anisotropic conductivity. On the other hand, recently characterized seismic metamaterials have demonstrated a unique ability to control propagation of surface Rayleigh waves in soils structured on a metre scale [4], also via dynamic anisotropy. Such an anisotropy is induced by evenly spaced boreholes in soil, which form a large scale crystalline structure when viewed from the sky. The band structure of the dispersion curves associated with elastic waves that are allowed to propagate through the array of boreholes leads to vanishing group velocity of Rayleigh waves in certain crystallographic directions near stop band edges, while it remains finite in other directions, and this leads to strongly anisotropic features. Analogies of models of diffusion in graphene oxide flakes and clay proposed in [3], suggest models of small scale diffusion metamaterials and large scale wave (seismic) metamaterials are two sides of the same coin, and that knowledge gained in the former field can be used for research advances in the latter field. Bridging design of mechanical metamaterials across the scales is in fact the main focus of the present topical article.

The contents of the article are as follows: we firstly introduce the concept of transformation crystallography and quasi-crystallography, and illustrate this with an example of transformed honeycomb (6-fold) and Penrose-type (5-fold) lattice in the plane. We then numerically investigate elastodynamic wave propagation with finite-difference-time-domain (FDTD) software SimSonic in large scale structured soils deduced from transformation crystallography. Our graphene-like seismic cloaks are also studied using a morphing algorithm [5]. We then consider similarities between invisibility cloaks for mechanical waves (counterpart of Pendry's electromagnetic cloak [6]) and thermal diffusion processes that have been theorized and experimentally validated by our research group at Institut Fresnel in Marseille and the research group of Martin Wegener at Karlsruher Institut für Technologie (note in passing thermal cloak controls in fact diffusion of high frequency phonons). We further use transmission electron microscopy images of flakes of a modified form of graphene (so-called graphene oxide, fabricated and characterized within the research group of Tania Puvirajesinghe at Institut Paoli-Calmettes in Marseille, for application in cancer therapy [3]), as a basis for numerical simulations of propagation and

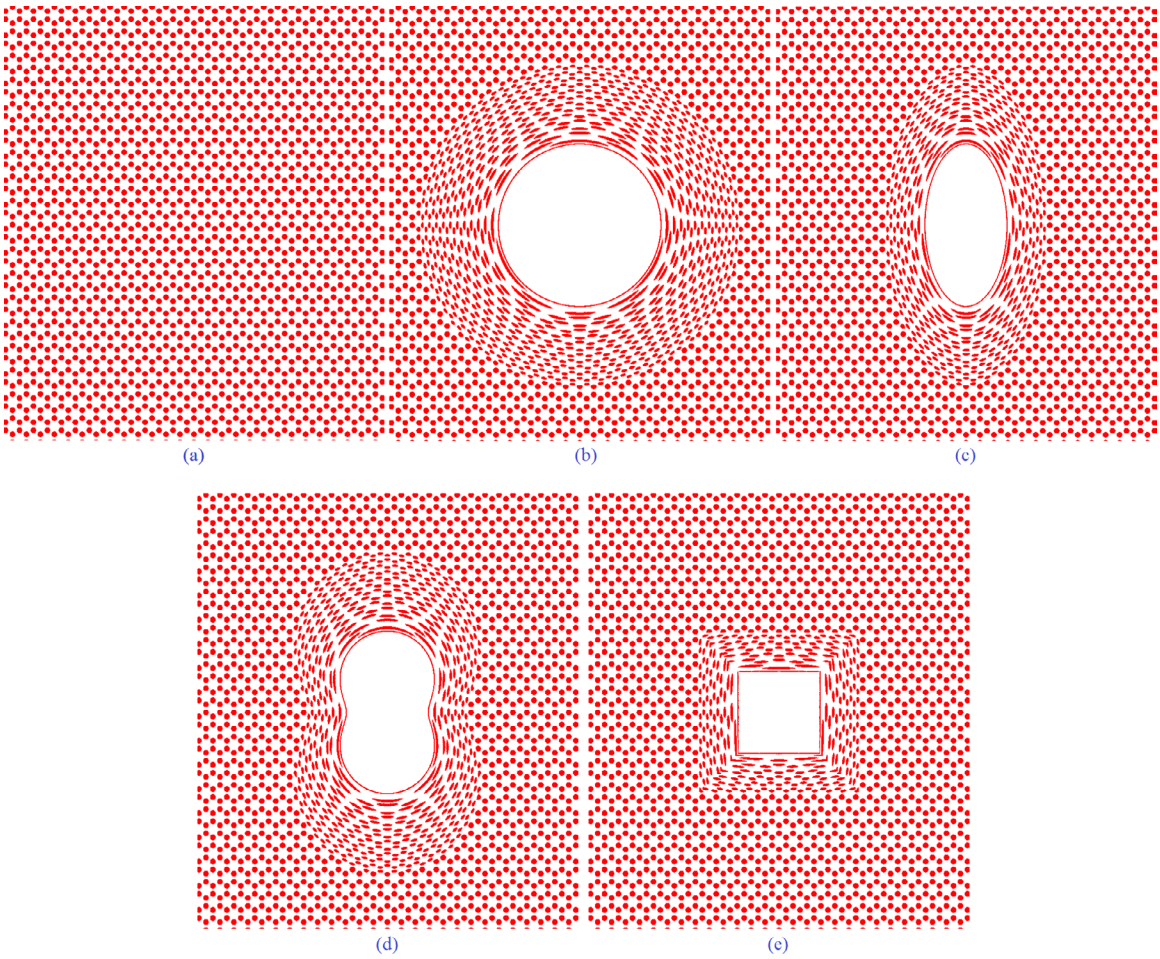

Figure 1. Graphene-like honeycomb lattice and transformed honeycomb lattices: (a) honeycomb lattice; (b)–(e) transformed honeycomb lattice with a circular cloak (b), an elliptic cloak (c), a peanut cloak (d) and a square cloak (e).

localization of elastodynamic waves within a scaled up version (by a factor of one million) of graphene flakes that can be considered as a biochemical counterpart of seismic metamaterial. We conclude our paper with a review of field experiments carried out by the engineering group, Menard, with results obtained and analyzed by the soil dynamic laboratory of Stéphane Brûlé in 2012, followed by some simulations of bridge vibration suppression with inertial resonators and the concept of transformed meta-cities. All throughout this article, we draw analogies across disciplines of crystallography, biology, wave physics and geophysics across different size scales.

2. Transformation crystallography and quasi-crystallography

In this section, we introduce new concepts of transformation crystallography (TC) and transformation quasi-crystallography (TQC). The power of this approach is illustrated in figure 1 with designs of circular (b), elliptic (c), peanut (d) and square (e) graphene cloaks obtained by the mapping of a hexagonal (honeycomb) lattice of points (a).

Before we explain how we do this, it is important to recall some counterintuitive properties of quasi-crystals, which had already been studied by mathematicians before Schechtman discovered them! A remarkable feature of the quasi-crystalline tiling patterns is that their assembly is obligatory non-local. Namely, in assembling the patterns, it is compulsory, in certain examples, to inspect the state of the pattern multiple atoms away from the point of assembly, so as to avoid defects (i.e. overlaps of motifs or empty spaces) when assembling the components together. In nature, a crystalline configuration is one that consists of the lowest energy status. With quasicrystal growth, the state of lowest energy is harder to reach than for periodic structures, and the optimal arrangement of the atoms cannot be unveiled by simply adding atoms sequentially with the assumption that each individual atom can solve its own minimizing problem. The state of lowest energy is the solution of a global minimization problem. Such tilings were previously studied by Sir Roger Penrose, who found many interesting mathematical properties related, as we will briefly discuss, to arithmetic and logic. It should be noted that quasi-crystalline substances also exhibit forbidden symmetries in three-dimensions such as icosahedral symmetry (these analogues of the Penrose tilings had been found by Robert Amman in 1975). Numerous mathematicians spent time on such hobbies, pastimes and everyday activities, and amongst them, the great number theorist and philosopher Bertrand Russell, the 3rd Earl Russell.

In the early 1970s, Penrose was considering the mathematical problem of tiling the Euclidean plane with a finite number

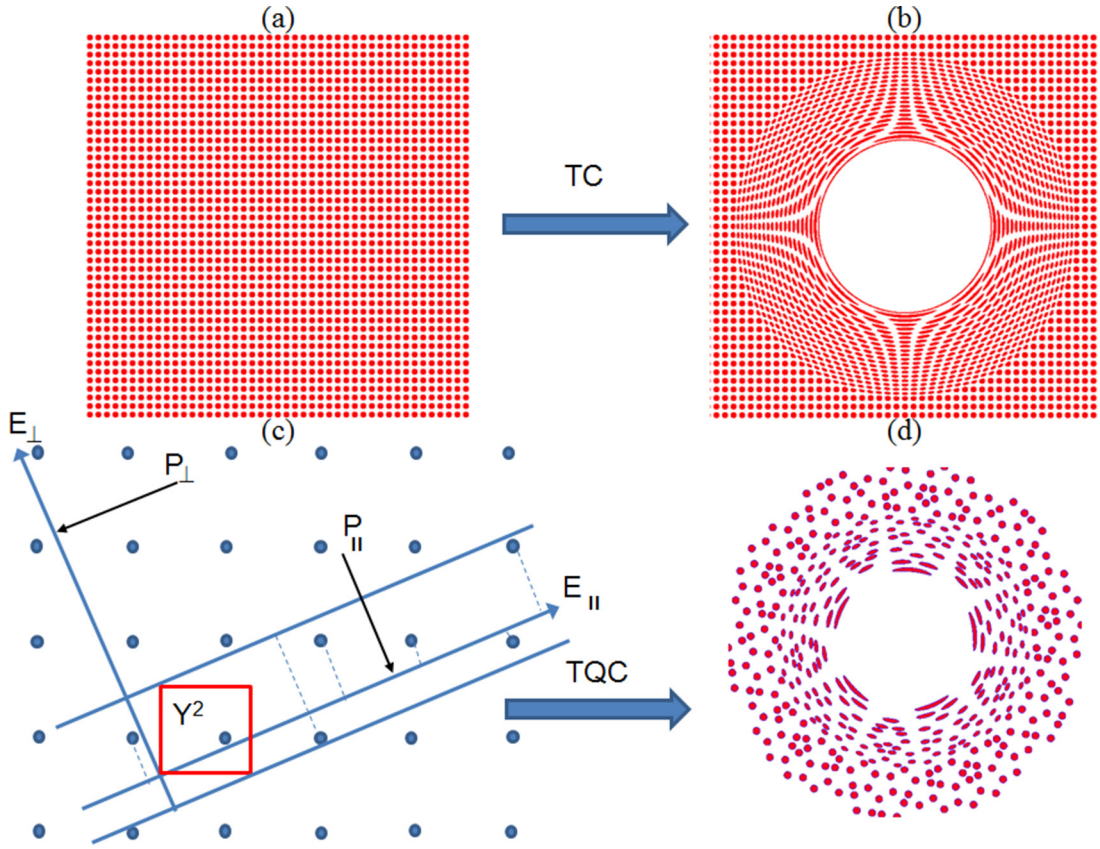

Figure 2. Principle of TC and TQC: (a) a mapping from a periodic square lattice onto (b) a transformed square lattice with a circular cloak using equation (1.1) with $a_1 = b_1$ and $a_2 = b_2 = 2a_1$; (c) cut and projection from a periodic upper dimensional space onto quasi-periodic (physical) space $E\|$. (d) Result of geometric transform equation (1.1) applied to $E\|$ in the case of a Penrose tiling.

of polygonal shapes. The initial task was to determine whether to cover the plane completely or not, without empty spaces (gaps) or overlaps, using just these shapes and no others. It is well-known thanks to the crystallographic restriction theorem that such tilings are possible using only squares, or only equilateral triangles, or only regular hexagons, but not only using regular pentagons. Alternative routes exist to tile the plane with single shapes such as irregular pentagons, but with a pair of shapes the tilings become more sophisticated. It is worth noting that more or less complex shapes can tile the Euclidean plane both periodically and non-periodically. However, can single or sets of tiles tile the plane in a non-periodical manner? In 1971, the American mathematician Raphael Robinson exhibited a tiling with six shapes, which tiles the plane only in a non-periodic fashion. Roger Penrose found in 1974 an aperiodic tile made of only two tiles.

In fact, tiling the Euclidean plane aperiodically with a single tile still remains an open question. A few potential paths to achieve this have been explored. For instance, Penrose suggested to assign the vertices of such a tile as points in the complex plane, and these points may be given as algebraic numbers. This proposal was supported by the Dutch mathematician Nicolaas Govert de Bruijn who proposed that such quasi-periodic tilings with one tile could be built thanks to a cut and projection method that was developed, amongst others, by the French Mathematical Physicists Michel Duneau and André Katz [5].

Let us briefly recall this cut and projection method, which is a special kind of geometric transform. Firstly, this mapping is not one-to-one (not an isomorphism), as we can see from the construction of a 1D quasi-crystal, say along a line $E\|$, in figure 2(c). Indeed, the quasi-periodic structure of the line $E\|$ is obtained as follows: take a strip generated by shifting a unit square $Y^2 =]0;1[^2$along $E\|$. It is clear that for almost all positions of the line $E\|$, this strip contains a unique broken line consisting of the lattice edges, which joins all the vertices inside the strip. If one considers the orthogonal projection $P\|$ of the broken line on $E\|$, this gives a tiling made of two tiles that are the orthogonal projections of the vertical and horizontal edges of the unit square Y^2. Consider now the slope of the line $E\|$ with respect to the canonical basis of $\Re^2$. It should be checked if the tiling is periodic and if the slope is a rational number. Duneau and Katz [5] have noted that any finite patch of tiles that belongs to a tiling appears infinitely many times in any tiling defined through a strip with the same irrational slope (this is the so-called local isomorphism property). To prove this property, one has to consider the line $E\perp$, orthogonal to $E\|$. Since a finite set of tiles in a given tiling is the projection of a finite broken line, then there exists a non-empty open set of translations in $E\perp$ that ensures the projection of the finite broken line remains inside the strip (the projection of the broken line on $E\perp$ is strictly smaller than the projection of the whole strip). Because the orthogonal projection $P\perp$ of the set of all pairs of integers $\mathbb{Z}^2$ on $E\perp$ is dense, Duneau and

Katz [5] deduced that there are infinitely many translations of $\mathbb{Z}^2$ which map the finite broken line inside the strip. The translations generate infinitely many copies of the initial patch of tiles. In the same way, one can show that any finite patch of tiles that appears in a quasi-periodic tiling appears in all tilings obtained from a cut and projection with the same irrational slope.

Secondly, besides from the local isomorphism, the mean distance between copies of a given patch gives rise to open mathematical questions. Intuitively the density of the copies of a patch in the quasi-periodic tiling should depend on arithmetical properties of the slope. Indeed, it can be seen that when the slope of $E\|$ is given by an algebraic number, the mean distance between two copies is proportional to the area of the patch. On the contrary, when the slope is given by a Liouville number (non-algebraic irrational number), the distance can quickly grow arbitrarily. It should be noted that if the unit square is replaced by any other square cell of the crystal lattice $\mathbb{Z}^2$ (say KY^2, where K is a positive integer), one can generate *ad libitum* new tilings constructed from the projections of the two edges of this supercell. This property is akin to self-similarity of the Penrose tilings i.e. each fragmented geometric shape can be subdivided in parts, which is almost (but not exactly) a reduced-size copy of the whole. More general strips also generate tilings involving a finite number of tiles via this projection method, and this led to a number of generalized cut-and-projection methods to generate miscellaneous quasi-periodic tilings.

As it turns out, one can easily generalize this method to higher dimensions. To get a quasi-periodic pattern in $\Re^n$ issued from a projection of a periodic pattern in $\Re^m$ ($m > n$), one has to consider the subspace $E\| = \Re^n$ and $E\perp$ its orthogonal subspace in $\Re^m$. The Penrose tilings are issued from a cut and projection of $\Re^4$ (or $\Re^5$) in $\Re^2$ and their 3D equivalents (the icosahedral structures) from a cut and projection of $\Re^6$ (or $\Re^{12}$) in $\Re^3$. This has important physical consequences as it is well known that the width of stop bands associated with a phononic crystal can be enlarged by the symmetry of the structure. The restriction theorem forbids to go over six-fold symmetry for crystals, but as one can infer from the cut-and-projection method, there is virtually no limit on the degree of symmetry one can achieve for a quasi-periodic structure. Because there is always a quasi-period of the same order as the wave wavelength (however large it might be), one can find arbitrarily low frequency stop bands [6, 7] in infinite photonic quasi-crystals, and similarly in phononic quasi-crystals [8]. Band diagrams of quasi-periodic structures can actually be computed using a generalized version of the Floquet–Bloch theorem in upper dimensional space [9]. Quasi-crystals hold strong promises for a range of photonic applications, especially those that require broadband, omnidirectional absorption of visible light [10], and we would like to stress that this is also true for mechanical waves, and among them earthquake waves propagating in soils structured in a quasi-periodic fashion.

Now that we have set the scene of periodic and aperiodic tilings of the plane and their links with geometric transformations, we can turn our attention to transformation crystallography and quasi-crystallography. Firstly, we recall the geometric transform for invisibility cloaks with an elliptical shape [11]:

$$\begin{aligned} f : (r,\theta) \to (r',\theta') &= (\alpha r + \beta, \theta), \\ \text{where } \forall 0 < r < R_2(\theta) &= \sqrt{a_2^2\cos^2\theta + b_2^2\sin^2\theta}, \\ \alpha(\theta) = (R_2 - \beta)/R_2, \beta(\theta) &= \sqrt{a_1^2\cos^2\theta + b_1^2\sin^2\theta}, \end{aligned} \tag{1.1}$$

which maps the area within the ellipsis of eccentricities a_2, b_2 onto an elliptical corona delimited by ellipses of eccentricities a_1, b_1 and a_2, b_2. Note that this transform is a straightforward generalization of Pendry's transform for circular cloaks [12, 13] that assumes $a_1 = b_1$ and $a_2 = b_2$.

Applying this geometric transform to the periodic structure shown in figure 1(a), we obtain figure 1(b) when $a_1 = b_1$ and $a_2 = b_2$ and figure 1(c) when $2a_1 = b_1$ and $2a_2 = b_2$. Figures 1(d) and (e) are obtained by making the angular dependence of r more complex. Such invisibility cloaks of arbitrary shapes described by Fourier series have been proposed in [14] and make use of

$$\begin{aligned} g : (r,\theta) \to (r',\theta') &= (\alpha r + \beta, \theta), \\ \text{where } \forall 0 < r < R_2(\theta) &= \sum_{k=1}^{n} a_2^k \cos(k\theta) + b_2^k \sin(k\theta), \\ \alpha(\theta) = (R_2 - \beta)/R_2, \beta(\theta) &= \sum_{k=1}^{n} a_1^k \cos(k\theta) + b_1^k \sin(k\theta), \end{aligned} \tag{1.2}$$

which maps the area within the closed curve of $R_2(\theta)$ onto a corona delimited by closed curves $R_1(\theta)$ and $R_2(\theta)$.

One can then deduce the metric tensor $\mathbf{T} = \mathbf{J}\,\mathbf{J}^{\mathbf{T}}/\det(\mathbf{J})$, in the transformed coordinates from the calculus of the Jacobian matrix $\mathbf{J}(r',\theta') = \partial(\mathrm{r},\theta)/\partial(r',\theta')$, its transpose $\mathbf{J}^{\mathbf{T}}$ and its determinant $\det(\mathbf{J})$. This metric $\mathbf{T}$ plays a prominent role in transform optics, and was already in use in computational electromagnetism twenty years ago [15, 16].

However, here we apply these transforms to crystalline and quasi-crystalline structures in order to generate a new class of transformed crystals and quasi-crystals.

In figure 1, we demonstrate the application of geometric transforms f (in (b) and (c)) and g (in (d) and (e)) to honeycomb lattice (a).

We obtain a collection of transformed lattices reminiscent of paintings by Victor Vasarely [17], a renowned artist for his artwork on optical illusions. It could be considered that Vasarely initiated transformation crystallography in an art form at approximately the same period as Victor Veselago introduced negative refraction [12]. Although the painter performed his geometric transforms with a pen and a piece of paper, the result of our computations appears to be strikingly similar to his paintings. It is important to precise at this point that other parallels have been drawn in [18] between complementary media and Vasarely's paintings. Therein, the crystallographic restriction theorem was invoked to keep a balance between overall positively and negatively refracting index materials as its application implies that only checkerboards with either rectangular, square or (equilateral) triangular cells can lead to perfect imaging devices associated with overall zero optical path-length. Although the authors of [18]

did not realize it at that time, they were essentially making use of transformational crystallography tools i.e. coordinate changes in periodic structures (in that case periodic sign-shifting checkerboards). An important feature that unfortunately falls beyond the scope of the present article is the application of the Floquet–Bloch theorem in transformed lattices, as already touched upon in [9] in the context of cut-and-projection method. A Floquet–Bloch wave function u would be of the form $u(f(\mathbf{x}+\mathbf{T})) = u(f(\mathbf{x}))\exp(\mathrm{i}f(\mathbf{k}\cdot\mathbf{T}))$, where $\mathrm{i}^2 = -1$, $\mathbf{x}$ is the position vector and $\mathbf{k}$ and $\mathbf{T}$ are respectively the Bloch and lattice vectors in the periodic reciprocal space and f is the mapping onto the transformed reciprocal space. One can easily envision the richness of band diagrams in transformed periodic structures that would be controlled by the function f.

Interesting extensions of classical mathematical theorems and their applications to physics of transformation crystallography will be addressed elsewhere.

3. Numerical illustrations of TC and TCQ with FDTD

The computer software SimSonic, which we use in this section to simulate propagation of elastic waves in crystals and transformed crystals is a freely available software designed by Emmanuel Bossy [19], which is based on finite-difference time-domain (FDTD) computations of the elastodynamic wave equations. SimSonic already serves as a tool for communities of researchers, teachers and students, and this package consists of several compiled programs and C source codes, freely available, under the GNU GPL license [20]. SimSonic solves the Navier equations in the following form:

$$\frac{\partial T_{ij}}{\partial t}(x,t) = \sum_{j=1}^{d}\sum_{i=1}^{d} C_{ijkl}(x)\frac{\partial v_k}{\partial x_l}(x,t) + \Theta_{ij}(x,t) \quad (1.3)$$

$$\rho(x)\frac{\partial v_i}{\partial t}(x,t) = \sum_{j=1}^{d}\frac{\partial T_{ij}}{\partial x_j}(x,t) + \Phi_i(x,t) \quad (1.4)$$

where C_{ijkl} is the rank-four symmetric elasticity tensor with d^4 [4] entries ($d = 2$ or 3), $T_{ij}$the rank-2 stress tensor and ν_i the particle velocity (vector) field. Besides from that, $\rho(x)$ is the density, $\Phi_i(x,t)$ and $\Theta_{ij}(x,t)$the force (vector field) and strain rate (rank-2 tensor) sources, respectively, with $x = (x_1,...,x_d)$ the space variable and $t > 0$ the time variable. In the present article, the dimension of the computation is $d = 2$. This means we consider the case of coupled in-plane pressure and shear waves. We consider a pressure source with a sine cube signal as shown in figure 3(a). This pressure wave is then converted into shear wave (and vice-versa) at each inclusion boundary of the (large scale) crystalline structure which we consider. In fact, since we assume the structured medium is invariant along the third dimension, in-plane and out-of-plane problems decouple. It is interesting to note that if we apply a geometric transform $f : (x_1,x_2) \to (x_1',x_2') = (f_1(x_1,x_2),f_2(x_1,x_2))$ to (1.3), then the transformed elasticity tensor has the form $C'_{ijkl} = \left(\frac{\partial f_1}{\partial x_1}\frac{\partial f_2}{\partial x_2} - \frac{\partial f_1}{\partial x_2}\frac{\partial f_2}{\partial x_1}\right)^{-1}\frac{\partial f_i}{\partial x_p}\frac{\partial f_k}{\partial x_q}C_{pjql}$, i,j,k,l,p,q = 1,2, with summation implicit on repeated indices as noted in [21]. This elasticity tensor does not have in general the minor symmetries. The transformed density simply has a factor of the determinant of the Jacobian det(**J**) of f, so remains a scalar quantity.

In figure 3, we show some snapshots of SimSonic computations that reveal the wave pattern of the seismic wave propagating within a graphene-like seismic metamaterial (a)–(c) with geometric parameters as in figure 1(a) and the same seismic wave propagating in the graphene-like seismic metamaterial after a stretch of coordinates has been made to achieve an elliptical cloak as in figure 1(c). It can be noted that this creates an exclusion zone in the center of the elliptical cloak, where the seismic wave magnitude is reduced by almost one half. For the bulk medium parameter, we consider a density of $10^3 kg\,\mathrm{m}^{-3}$ (very soft soil), whereas the density of inclusions is $10^4 kg\,\mathrm{m}^{-3}$ (denser soil). These extreme parameters were chosen as we wanted to test the effect of a high-contrast in density on the wave propagation, inspired by 22,23. Note nonetheless that columns of concrete typically have density about $2.5\times10^3 kg\,\mathrm{m}^{-3}$ and thin-walled steel tubes have density about $7.8\times10^3 kg\,\mathrm{m}^{-3}$, so our parameters are in actuality achievable. The coefficients of the elasticity tensor used for the bulk medium (e.g. soft soil with an assumption of isotropic homogeneous medium) are given in Voigt notation

$$\begin{bmatrix} \frac{\partial T_{11}}{\partial t} \\ \frac{\partial T_{22}}{\partial t} \\ \frac{\partial T_{12}}{\partial t} \end{bmatrix} = \begin{bmatrix} C_{11} & C_{12} & 0 \\ C_{12} & C_{22} & 0 \\ 0 & 0 & C_{66} \end{bmatrix} \begin{bmatrix} \frac{\partial v_1}{\partial x_1} \\ \frac{\partial v_2}{\partial x_2} \\ \frac{\partial v_2}{\partial x_1} + \frac{\partial v_1}{\partial x_2} \end{bmatrix} \quad (1.5)$$

and they are $C_{11} = C_{22} = 0.25\,\mathrm{GPa}$, $C_{12} = 0.25\,\mathrm{GPa}$, $C_{66} = 0$ in soil and $C_{11} = C_{22} = 25\,\mathrm{GPa}$, $C_{12} = 25\,\mathrm{GPa}$and $C_{66} = 0$ in inclusions (denser soil e.g. concrete with an assumption of isotropic homogeneous medium). Note that we consider a rather high Poisson ratio (close to 0.5), but we checked that increasing value of $C_{66} = 0$ in inclusions does not affect much the simulations. What prevails is that we have a large contrast between elasticity tensor in soil and inclusion to enhance wave control, just like what [22, 23] and other work on homogenization theories suggest.

The transformation underpinning the cloak's design is carried out on a region of area $225\times131\,\mathrm{m}^2$ consisting of 50×50 hexagons with circular inclusions located at each vertex. The radius of each inclusion is 0.5 m and their spacing, center-to-center, is 1.5 m (so inclusions are close to touching, so as to increase their interaction). Each simulation runs for 1000 ms with a snapshot taken every 10 ms. The computational domain is a rectangle of side lengths $898.2\times524\,\mathrm{m}^2$ and it encompasses the transformed area (the cloak).

With all these assumptions, we satisfy the stability condition (CFL condition, from the initials of the German American mathematicians Richard Courant, Kurt Friedrichs and Hans Levy) for the numerical scheme:

$$\Delta t \leqslant \frac{1}{\sqrt{d}}\frac{\Delta x}{c_{\max}} \quad (1.6)$$

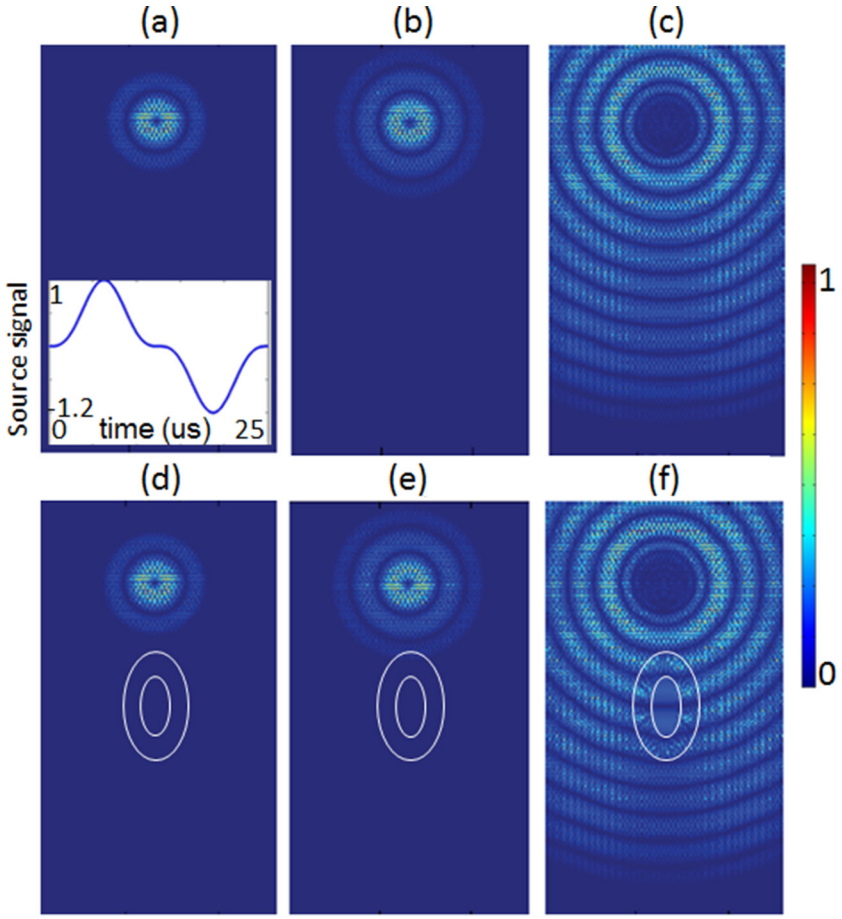

Figure 3. Numerical simulations (SimSonic software) for a point force oscillating out-of plane (x_3-direction orthogonal to (x_1, x_2) plane of computation) at frequency 10 Hz generating a seismic wave propagating in a graphene-like seismic metamaterial (representing soft soil with columns of denser soil arranged in a honeycomb fashion) like in figure 1(a) (upper panel) and the same with an elliptical cloak (highlighted with white boundaries for clarity) like in figure 1(c). Snapshots at $t = 100$ ms ((a) and (d)), $t = 150$ ms ((b) and (e)) and $t = 570$ ms ((c) and (f)). Note the reduced wave amplitude in the center of the cloak in (f) compared to (c). The center to center spacing of columns is 1.5 m and their diameter is 0.5 m in (a)–(c), while in (d)–(f) the mapping has stretched these distances like in figure 1(c). Insert in (a) shows the chosen wave signal (sine cube). Linear color scale ranges from dark blue (vanishing) to red (maximum) displacement field.

where $d = 2$ is the space dimension, $\Delta x = 0.2$ m and $\Delta t = 10\mu$s are the space and the time discretizations, $c_{\max} = \sqrt{C_{11}/\rho} = \sqrt{E(1-\nu)/((1+\nu)(1-2\nu))} = \sqrt{25 \times 10^9/10^4} = 1580\,\mathrm{ms}^{-1}$ is related to the speed of pressure waves in denser soil.

In figure 4, we show similar snapshots for square (a), circular (b) and peanut (c) seismic graphene-like cloaks at 570 ms. In all three cases the displacement field has smaller amplitude within the exclusion area (seismic protection) than in figure 3(c): according to integral of out-of-plane displacement computed over the surface of the invisibility region (i.e. center of cloak) in figures 4(a)–(c) normalized by same in honeycomb lattice in figure 3(c), about half of the seismic wave energy is smoothly detoured around the cloak. We refer the reader to supplementary material for movies (stacks.iop.org/JPhysCM/29/433004/mmedia) showing there is indeed wave reduction inside the exclusion zone from 500 ms to 780 ms i.e. until the seismic wave has crossed the cloak. Importantly, there is virtually no reflection of the seismic wave by the cloak, hence protection of a given infrastructure with such a cloak would not be deleterious for surrounding infrastructures, unlike for the seismic shield discussed later on in this article.

In figure 5, we propose a concept of Penrose-like seismic cloak, which is based on a geometric transform in a Penrose lattice. The latter has been designed using cut-and-projection method, as discussed in section 2. However, we numerically observed that the level of protection displayed by this cloak is less prominent than for the graphene-like cloak in figures 5 and 6 for the same source oscillating at 10 Hz, so we report here the result of SimSonic computation when the source oscillates (out of plane i.e. along x_3) at frequency 20 Hz, in which case seismic protection is achieved in the (x_1, x_2) plane (in-plane seismic signal). We nevertheless are convinced that transformed quasi-periodic lattices offer a very promising route towards seismic cloaks, as one can generate such lattices from cut-and-projection of periodic lattices in higher-dimensional spaces (5 and 12 for instance) and then further choose the transform allowing for designs of quasi-periodic lattices (with 5-fold and 12-fold symmetries for instance) with an exclusion area for any given shape.

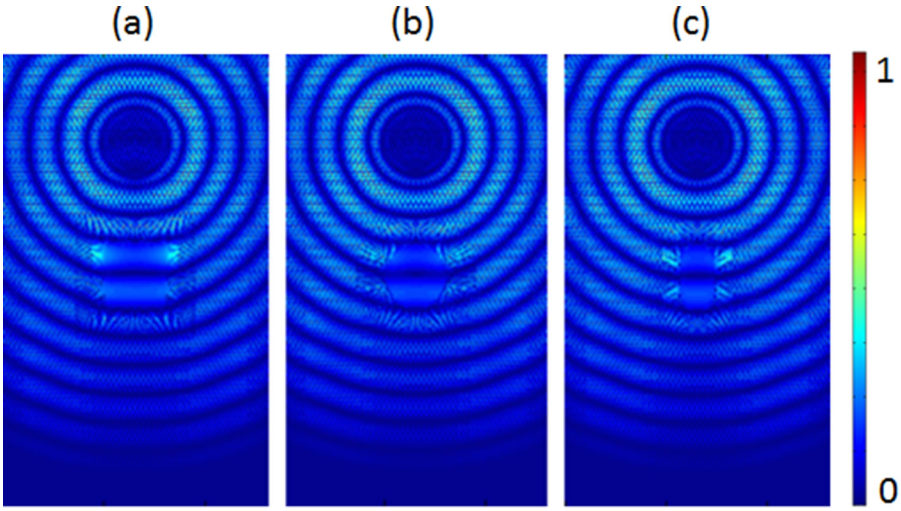

Figure 4. Numerical simulations (SimSonic software) for a point force oscillating at frequency 10 Hz generating a seismic wave propagating in a graphene-like seismic metamaterial (soft soil with columns of denser soil) like in figure 1(e), a square cloak (a), figure 1(b), a circular cloak (b), and figure 1(e), a peanut cloak (c). Snapshots are taken at $t = 570$ ms. Linear color scale ranges from dark blue (vanishing) to red (maximum) displacement field.

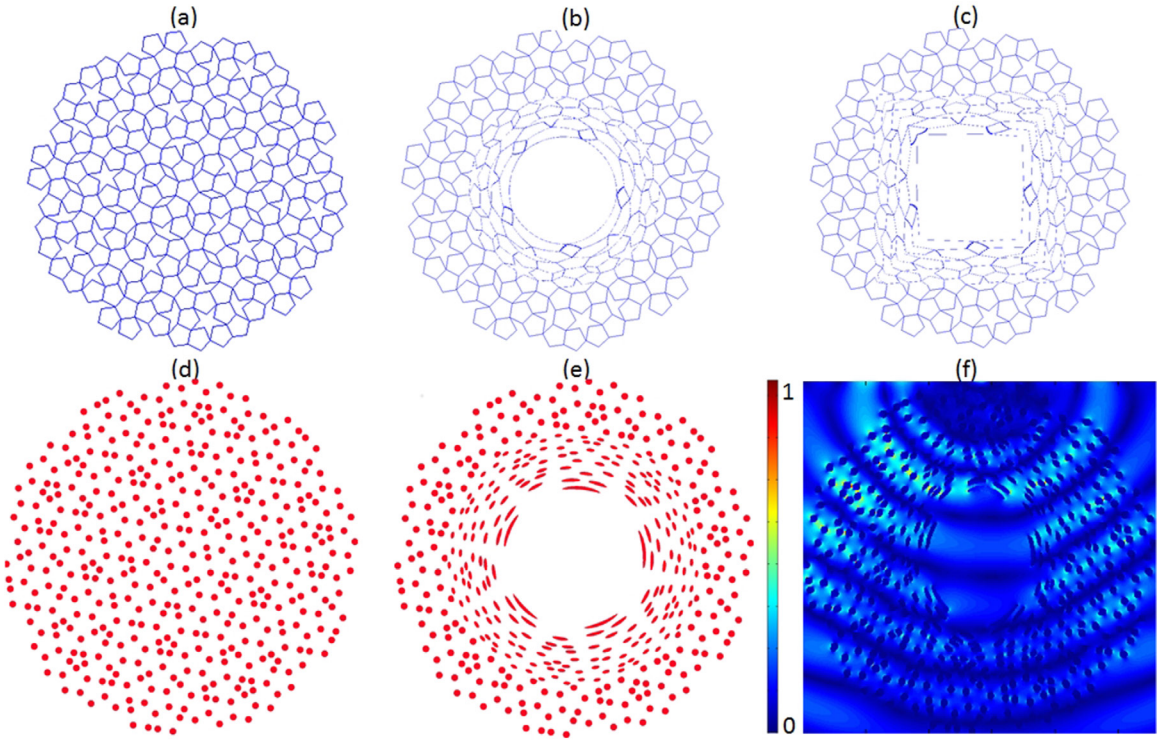

Figure 5. Transformed Penrose lattices (five-fold symmetry): (a) Penrose lattice from cut-and-projection method; (b) and (c) transformed Penrose lattice with a circular cloak (b) and a square cloak; (d) and (e) same with vertices only; (f) numerical simulation (SimSonic software) for a point force located just above the cloak and oscillating at frequency 20 Hz along x_3 generating a seismic wave propagating in Penrose-like seismic metamaterial (soft soil with columns of denser soil). Linear color scale ranges from dark blue (vanishing) to red (maximum) displacement field.

Let us now move to the morphing technique [24, 25], which can be viewed as a geometric transform of an elastically deformable model [24], and thus bears some resemblance with transformational physics techniques although in the present case, it is based on control points rather than an explicit mathematical formula, so one might be tempted to call this an 'inverse engineering geometric transform'.

4. Morphing and seismic metamaterials

The late 1980s saw a rise in the popular media use of the effect called 'morphing' which amounts to transforming an image into a second image via a series of intermediate images. This computer graphic technique, which rose to fame thanks to the film *Willow* of Ron Howard and the musical video clip *Black or*

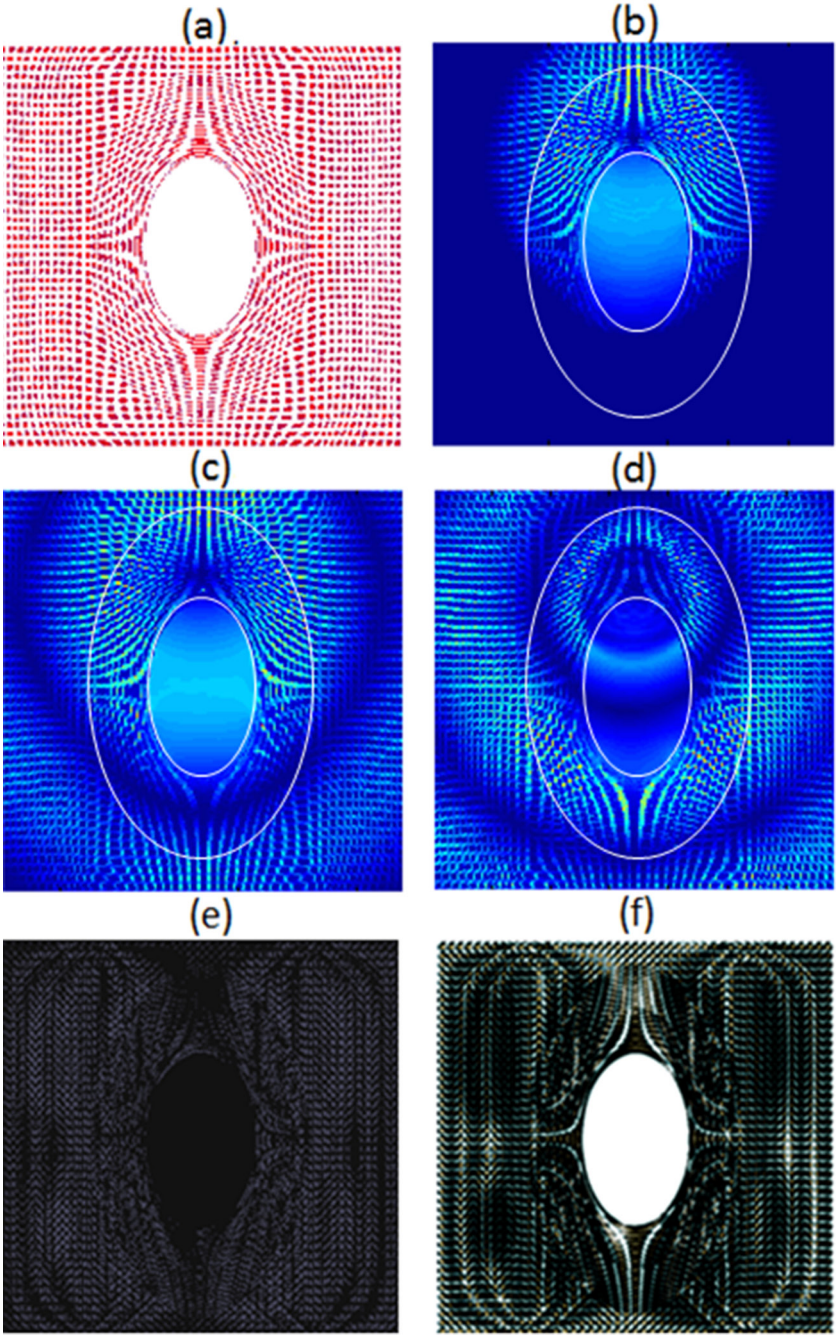

Figure 6. Seismic cloak (highlighted with white boundaries for clarity) generated by 75% morphing from figures 2(b) to (c); (a) is the resulting stretched image; (b)–(d) snapshots at 100 ms (b), 200 ms (c) and 520 ms (d) from SimSonic computations for a source at frequency 20 Hz. Blue pixels for soft soil and red pixels for denser soil. Note that protection becomes more effective at 520 ms, at which time step quantification of protection reaches around 50%. (e) Difference in gray scale between figure (a) and elliptical cloak with 75% of eccentricity corresponding to 0.0849 in L^2 norm; (f) same as (e) for SSIM index [30] that gives 0.4461 of image difference. We point out that for error estimates in numerical results, the L^2 norm is the natural tool of choice.

White of Michael Jackson could be helpful in transformation physics and wave simulations. Indeed, morphing and transformational optics bear some resemblance, since the two of them are underpinned by coordinate changes. Photonic researchers use coordinate changes to create artificial media *ex nihilo* (usually one maps vacuum onto a heterogeneous anisotropic medium). In this way, researchers achieve control of light trajectories in transformed (metamaterial) media [11–15]. In the following paragraphs, we would like to show that morphing can be used as a design tool for certain types of metamaterials via a novel concept of transformational crystallography. By adopting such a radically different viewpoint (we no longer map free space on a metamaterial, but rather a periodic or aperiodic crystal), we unveil new classes of transformed media, and even intermediate transformed media (through morphing). Interestingly, computer assisted science becomes unavoidable for researchers from miscellaneous fields, including photonics, geophysics and biological sciences, and we believe

morphing will find a growingly important place by their side in the coming years. In the sequel, we propose applications of morphing techniques as a design tool for transformational crystallography.

4.1. Principle of morphing

Morphing literally speaking is an image transformation (underpinned by coordinate changes) that includes interpolation of colors: the colors of the source's image progressively fade away to reveal the colors of the destination's image. To summarize, morphing is based on a double interpolation, both on shapes and on colors, between two images. There are many freeware softwares that are capable of doing just this, however, here we work with Sqirlz Morph [26].

4.2. On the usefulness of control points

Whatever the choice of the morphing technique used, 'control points' need to be selected manually and assigned by the user, in the source and the destination images. These control points specify the important features of the two images, and should be such that each control point in one image corresponds to one control point in the second image (for a one-to-one mapping). Control points are essential for the shape's transformations. Their placement drives the series of intermediate images between the source and destination images. For instance, control points should neither be aligned nor too close to each other as morphing preserves proportions, and their number chosen judiciously (too few control points will produce a superposition of the source and destination images and too many control points might produce awkward transformations). Therefore, choosing the location of the control points requires consideration of many parameters, which means that this step is not easily amenable to automation [24, 25] (though this is a potential obstacle for acceleration of numerical simulations through morphing [27]). This is a pivotal feature in morphing assisted transformation crystallography as human intervention leads to a subjective result: morphing will mostly lead to transformed media that are envisioned by the user.

4.3. Application to design of seismic metamaterials

Let us consider panel (b)—a circular cloak—in figure 2 and further generate an elliptical cloak from the same square lattice in panel (a). We would like to apply the morphing algorithm between the circular and elliptical cloaks. We emphasize the importance of placing control points at the barycenters of transformed red inclusions in the two images, which leads to figure 6(a). The reader can easily create other designs with Sqirlz Morph, just by placing control points in specific positions. Also, it should be noted that when the number of control points is too small or too large the result of morphing can be quite surprising, the reader can also experience this. By doing so one can generate beautiful patterns that can serve the purpose of seismic metamaterials reminiscent of artwork of Vasarely [17]. In the present case, we have designed a seismic cloak, using Pendry's transform [12], which serves our purpose. One can see that among the three snapshots taken from SimSonic simulations of an elastic wave propagating in soft soil (blue) with denser inclusions (red), the last one (d) at 520 ms shows a reduction of the elastic field magnitude in the exclusion zone of the cloak. We have checked that this remains the case at higher time points. However, at shorter times, it appears from (b) and (c) that the cloak is not yet efficient for protection. Nevertheless, one notes that the elastic field displacement is nearly constant in the exclusion zone and the soil therein moves almost like a rigid body, which suggests some kind of trapped fundamental mode of a stress-free cavity, as already observed in similar situations [28, 29]. Importantly, invisibility is already achieved at short times: a velocimetre placed behind the cloak would not detect any significant change of the seismic signal compared with the case where there is no cloak: the wavefront is almost circular and its amplitude is close to that of the wave propagating in the medium shown in figure 2(a) i.e. without cloak.

It is illuminating to compute the difference between 75% morphing (figure 6(a)) and direct geometric transform between the circular cloak in figure 2(b) and its elliptic counterpart (not shown, see supplemental material) when we consider an elliptical cloak of eccentricity ¾ to that in arrival image (not shown). Figure 6(e) shows that difference in L^2 norm computed with the formula

$$F = \sqrt{\frac{1}{N}\sum_{i=1}^{N}\left(\frac{K_i}{255}\right)^2} \tag{1.7}$$

(where the sum is taken over all the pixels $(K_i)_{=1,..,N}$ in the image and each pixel K_i has a value between 0 and 255) is less than 1% (for images converted in grayscale). Importantly, this formula only works for grayscale images (when applied to color images, one has to consider a vector valued function K_i with three components for red, green and blue colors, respectively, and the approach breaks down). Interestingly, the structural similarity (SSIM) index [30], which is a method used for predicting the quality of digital images perceived by a human eye, gives a difference of almost 45%. Actually, one can see that figure 6(e) is almost black (vanishing L^2 norm), whereas figure 6(f) clearly has striking instantly recognizable differences. SSIM is based on a complex mathematical formula that can be found in [30], but roughly speaking it is a mathematical model that quantifies the degradation of an image via a perceived change in structural information.

We do not find such antagonistic results between L^2 norm and SSIM in our previous investigations of morphing applied to transformation optics [27], which were based on coordinate stretches in invisibility cloaks surrounded by homogeneous medium. In the present case, the homogeneous bulk is replaced by a periodic cladding, so the coordinate stretch is much more challenging to mimic with morphing (as one has to place many control points in the periodic cladding). We believe we are in presence here of configurations where these two estimates for image differences (L^2 norm and SSIM [30]) cannot be reconciled (a whole class of transformational

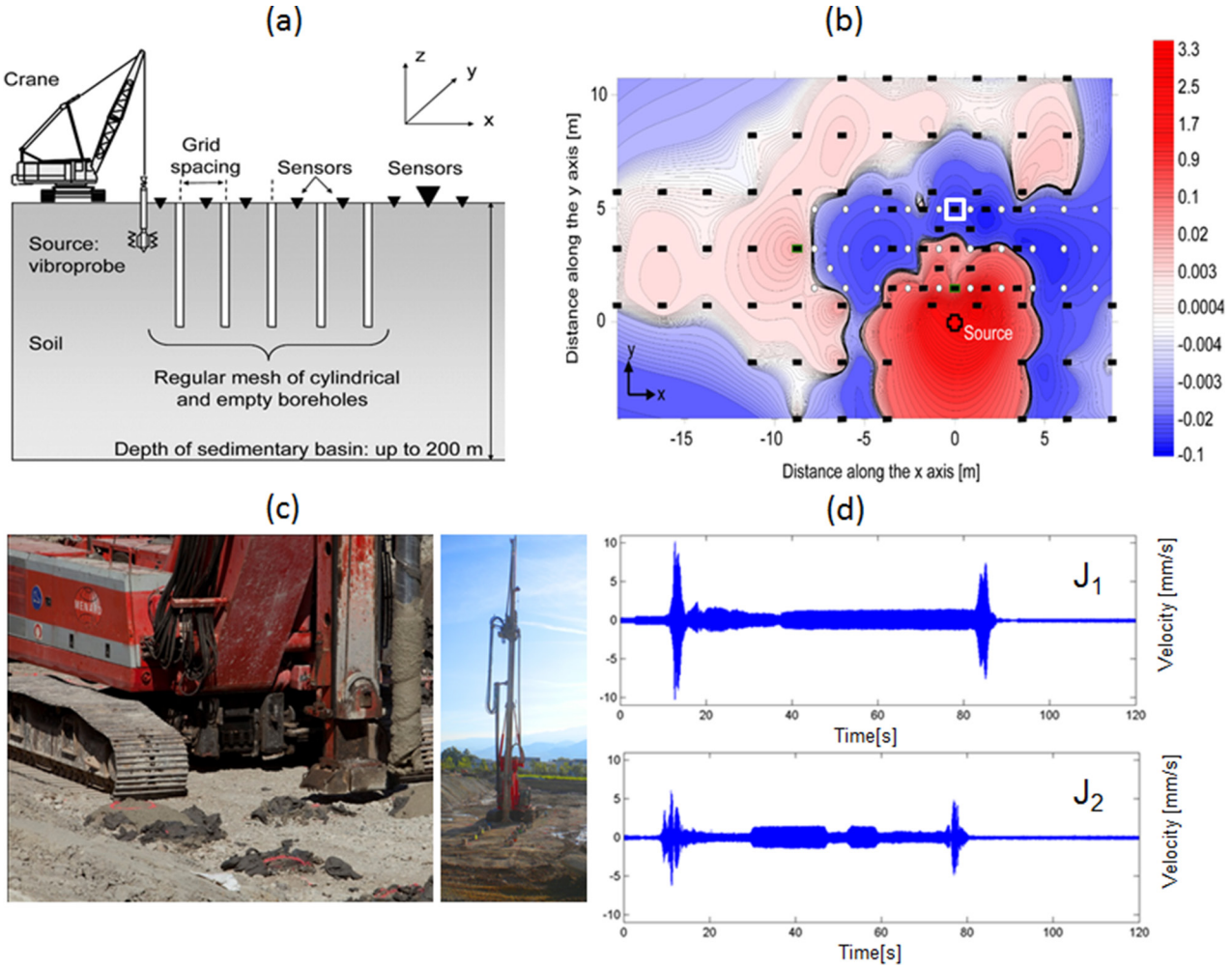

Figure 7. Scheme of the 2012 field test experiment conducted by the Ménard company in Grenoble (a): an oscillating probe generates acoustic waves at 50 Hz in front of a mesh of cylindrical boreholes. An array of sensors monitors the intensity of the waves at various positions. Experimental results (b): the map (black rectangles: sensors; white circles: boreholes; red-cross with black boundaries: source) plots the difference of energy J_2–J_1 after (J_2) and before (J_1) drilling the boreholes. The dark blue region behind the holes indicates that the presence of the mesh of boreholes results in a decrease of elastic energy transmitted to that area. The red region indicates the area close to the source in which the wave intensity increases because of reflection. (c) Photos of experiment crane with close-up on crane used to drill boreholes and used as source (left) and overview of site (right); (d) recorded data by sensor (vertical particle velocity versus time) located at black rectangle highlighted by white boundary in (b), before (J_1, upper panel) and after (J_2, lower panel) drilling the boreholes. One notes the reduced velocity in J_2. Credit: Brûlé *et al* [4] and (c) courtesy of Ménard.

crystallography based images would indeed face the same fate). However, regarding numerical simulations, it is usual to use L^2 norm for error estimates, and we have checked that FDTD simulations of elastic waves propagating in morphing based medium in figure 6(a), see snapshots in figures 6(b) and (c), and corresponding snapshots for elastic waves propagating through the transformed medium from 75 percent stretching in figure 2(b) and its elliptic counterpart, are almost identical (less than one percent of difference in L^2 norm).

4.4. Field test experiments in seismic metamaterials

We now investigate the similarities between models of nano-scale photonic and phononic crystals, and metre-scale seismic metamaterials, as introduced in recent papers [4]. We recall in figure 7 the scheme of the first large scale experiment on seismic metamaterials (left panels (a) and (c)), which was conducted by the dynamic soil laboratory team of Stéphane Brûlé at the Ménard company in August 2012. The experimental data (right panels (b) and (d)) shows that when a seismic source oscillates at a frequency inside the stop band of the periodic structure, here 50 Hz, Rayleigh waves become reflected, just like a photonic crystal does for light.

A keen observer of civil engineering works can observe that certain artificial and buried structures in the soil seem to be a translation of crystallographic lattices (figure 8). The common structure is made of vertical and cylindrical inclusions (concrete, steel, etc) implemented in the soil, reproducing a square meshing in the plan $(0, x, y)$. To achieve an improvement in the density of soil strengthening, the equivalent of a face-centered cubic system can be observed too in plan $(0, x, y)$ with vertical concrete rods.

However the primarily objective of these worksites is to make the soil more resistant to shear strains induced by a

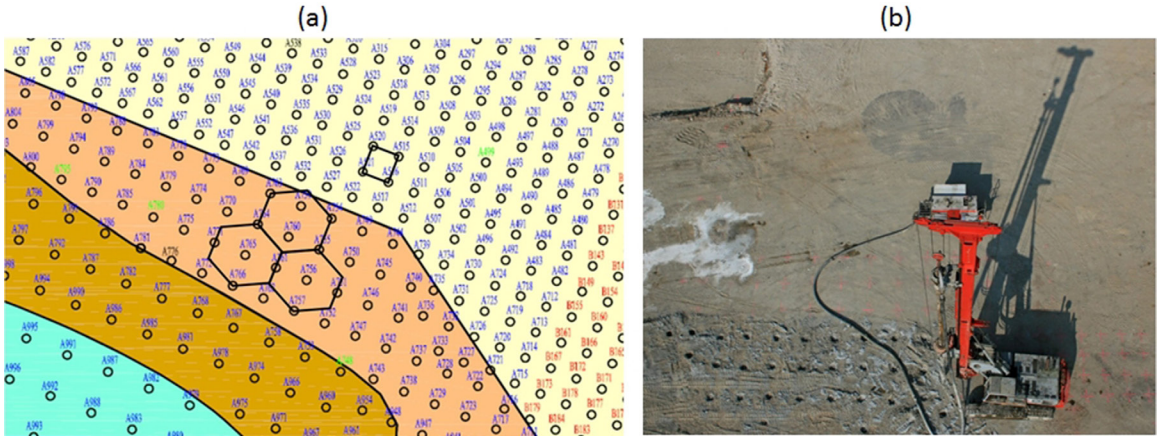

Figure 8. Illustration of high-density ground reinforcement with vertical, cylindrical lime inclusions arranged in a square grid (b). The horizontal spacing is comprised between 1.3 and 2.0 m and the diameter of the inclusions is around 0.3 m (courtesy of Ménard). (b) The nodes of the grid could be design in agreement with the graphene-sheet structure.

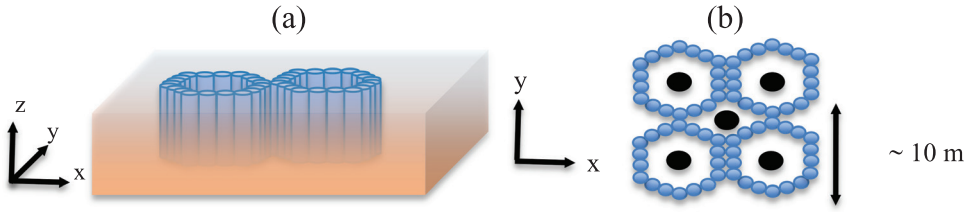

Figure 9. Principle of a honeycomb (a) and 'quasi-honeycomb' (b) meshes made of jointed concrete inclusions (blue) and viaduct piles (black) in the soil (brown). Piles and soil-cement mixed columns [35] would act as protection for viaduct piles.

simplified representation of the seismic disturbance, i.e. considering that the more devastating component of the seismic signal correspond to the horizontal component of the body shear-waves. The fascinating concept carried out by several authors and that has boomed in the past few years is the introduction of the concept of photonic and phononic crystals in geophysics. As aforementioned, in August 2012, a first full-scale field experiment was realized with a non-sub wavelength 2D square grid of vertical empty cylindrical holes disturbed by a 50 Hz source, showing a characteristic Bragg's effect [4] reminiscent of stop band properties of photonic crystals [31, 32] put forward by Eli Yablonovitch and Sajeev John in 1987. Such periodic dielectric structures, that were also studied by Stokes and Rayleigh towards the end of the nineteenth century [33], and by Bykov and Ohtaka in the 1970s [34, 35], allow for spontaneous emission of light and almost total reflection of light. The idea proposed, and experimentally demonstrated in [4], is to simply scale up photonic crystals (which have typically an array pitch on the order of a few hundredth of nanometres) by a factor of 10^4 to 10^5, so as to reflect surface seismic wave a few metres in wavelength in structured sedimentary soils.

Though this idea initially appears as far-fetched, leading to initial skepticism from certain research groups, it is now appears to be widely accepted, and further, experiments have been by the geophysics team of Philippe Roux on stop band properties of forest of trees [36] in the tracks of large-scale seismic metamaterials and tested by Menard engineering group [4]. Another interesting way to protect an area is actually to convert surface Rayleigh waves into shear bulk waves, which is precisely what the metawedge does [37]. Such concepts of forbidden propagation bands might also find applications in design of bridge piles [38], as we shall see.

Apart from these features, the soil-liquefaction remediation in the case of earthquake could be achieved by incorporating a mesh of vertical concrete walls (shear-walls), or jointed piles or inclusions in the soil as depicted in figure 9 (left). One can imagine to reproduce thus the graphene structure. It can be noted that in 2002, Takemiya and Shimabuku [38] suggested the realization of a 'semi-honeycomb pattern' around viaduct piles (figure 9(b)) with soil-cement mixed columns. Their objective was to improve the global stiffness without immensely modifying the mass of the system. These buried structure are expected to work not only for reducing the seismic input thanks to the cell stiffness but also for absorbing seismic energy by self-damaging in case of severe earthquake.

5. Graphene flakes as bio-metamaterials for control of mass diffusion

In this section, we aim to begin to bridge concepts of seismic wave physics and diffusion phenomena, in the present case mass diffusion (note that mass diffusion is governed by a Fick's equation whereas heat diffusion is governed by Fourier's equation), to broaden our horizon of the design of cloaks. In figure 10, one can see two numerical simulations in the upper panel, placed next to each other in order to emphasize the similarities (and differences) between the wave and diffusion patterns. In both cases, a layered cloak

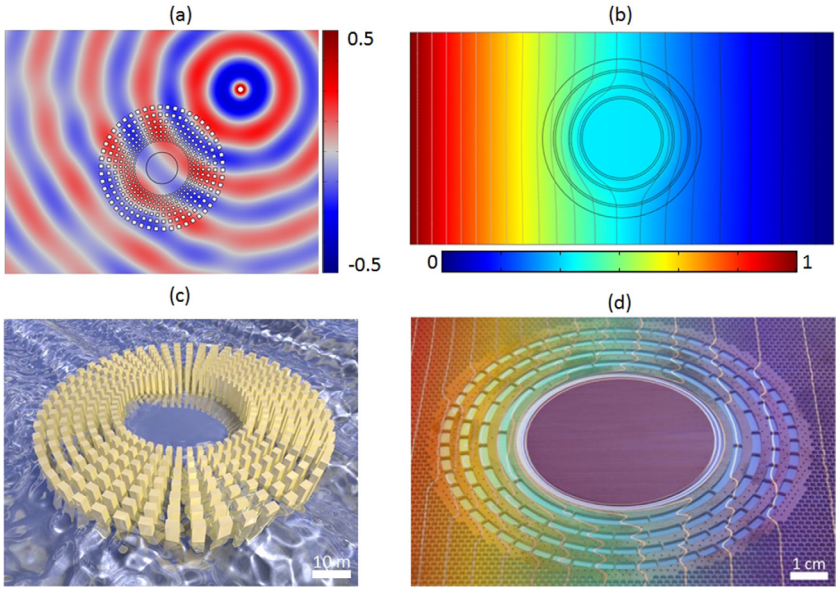

Figure 10. Mechanical versus thermal cloaking for invisibility and protection; (upper panel) numerical simulations for the propagation of a Rayleigh-like wave in a plate of thickness 40 m generated by a time-harmonic point source of frequency 10 Hz located in the close vicinity of a layered cloak (based on a scaled up version of cloak by Farhat *et al* [39]) of diameter 500 m (a) and diffusion of heat (from left to right) in a layered cloak (b) of diameter 10 cm; (lower panel) artistic view by Tolga Ergin (Martin Wegener's team at KIT) of ocean wave cloak (based on a scaled up version of cloak by Farhat *et al* [40]) (c) that works in the same manner has the earthquake cloak (rigid pillars have the same geometry whether they are plunged in soil or water) and result of Robert Schittny (Martin Wegener's team at KIT) experiment on control of heat diffusion [41] in false colors (d); note that the wave amplitude (left) and heat magnitude (right) vanish in the center of the wave and diffusion cloaks. Adapted figure with permission from [41], Copyright 2013 by the American Physical Society.

simultaneously leads to invisibility and protection. From the seismic wave pattern in figure 10(a), which is a numerical simulation based on a scaled up version of [39], it appears clear that the center of the cloak is the ideal location to build a monument: the wave magnitude vanishes there. Similarly, from the chemical concentration distribution in figure 10(b), one could envision some delayed drug diffusion if the drug is placed in the center of the biocloak: the inner boundary of the cloak acts like a barrier for chemical species, it is difficult to get inside the invisibility region and by reciprocity the drug can be concentrated in this region.

These two cloaks, which are of very different scales (tenths of meters for the seismic cloak and tenths of nanometers of the drug diffusion cloak), have been somewhat already experimentally validated, see lower panel for an illustration by Tolga Ergin (group of Martin Wegener at Karlsruhe Institute of Technology, that also produced magnificent computer based photorealistic views of carpet cloaks [42]) of the protection offered by an ocean cloak, which is a scaled up version of the water wave cloak designed and tested experimentally in [40].

The experimental measurements of Robert Schittny (Wegener's group at KIT) for a thermal cloak studied in the time domain in [41], see figure 9(d), can be used to predict what can be achieved for control of drug diffusion with concepts developed in [43]. In the same way, if one finds it legitimate to draw analogies between water waves (ocean cloak), surface Rayleigh waves (seismic cloak) and heat and mass diffusion (biophysics cloak), the latter being solutions of the Fourier–Fick equation:

$$\sum_{i=1}^{d} \frac{\partial}{\partial x_i} \sum_{j=1}^{d} \kappa_{ij}(x,t) \frac{\partial}{\partial x_j} H(x,t) = \frac{\partial}{\partial t} \left(\rho(x,t)\, c(x,t)\, H(x,t)\right) \tag{1.8}$$

where κ_{ij} is the conductivity tensor, which under geometric transform, as shown in [43] takes the form $\kappa' = \mathbf{J}\kappa\mathbf{J}^{\mathbf{T}}/\det(\mathbf{J})$ and ρ and c represent respectively the density and specific heat in the case of heat, a product which is equal to 1 for the case of mass diffusion, then another interesting parallel can be drawn between the biophysics at the nanoscale and the geophysics at the meter scale. At a nanometer scale, the diffusion of different types of macromolecules in matrix-based context is highly studied and is the basis for important biological measurements techniques such as fluorescence recovery after photobleaching and fluorescence correlation spectroscopy [44, 45]. It has recently been shown that the structures of materials such as graphene and derivatives of graphene, graphene oxide can be exploited as molecular filters allowing the permeation of ions of certain hydrated radii to pass through [46, 47]. Matrix structures have already been describing which combine graphene and clay based structures, which both can be modelled to use condensed matter theory and effective medium approaches to describe the movement of aqueous media [43, 48–50]. Graphene-matrices using therapeutic molecules for human therapy have also been developed [3]. Though graphene materials were initially used simply for chemical conjugation purposes, it has now been shown that graphene is able to produce retardation effects which are useful in the development of controlled or slow-release drug formulas [43, 51]. This is an important health application as

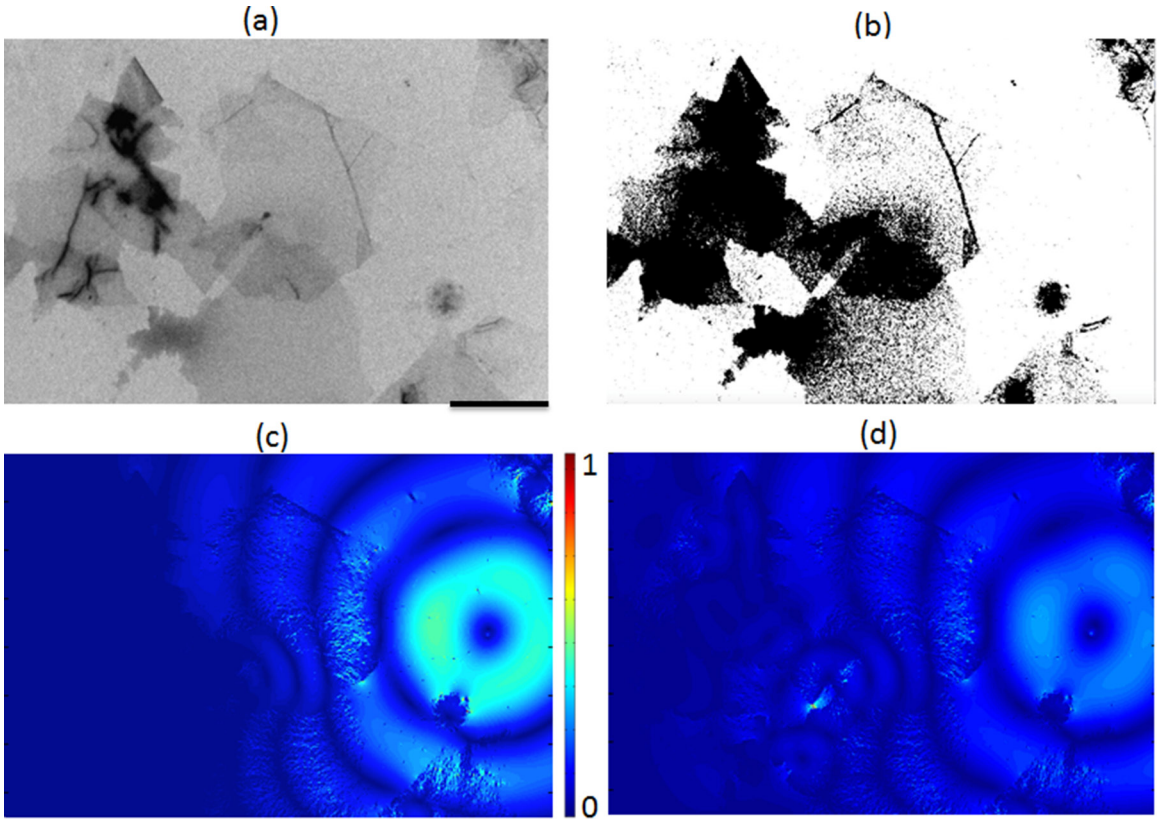

Figure 11. Seismic lens as a scaled up version from TEM images: (a) TEM images of a modified form of graphene, graphene oxide (GO). Images are acquired using a Morgagni FEI 80KV Camera digital View III Olympus camera. Multiple sheets show a sharp increase in the contrast when many GO flakes are stacked together, thereby substantially increasing the gray scale of the images. Scale bar is 2 μm. Dark regions correspond to folded layers of GO sheets, which are capable of folding over though remaining intact thanks to their high flexibility; (b) same image after treatment, with white pixels for soft soil and black pixels for denser soil (image with 1139 pixels $\times$ 750 pixels and each pixel is 0.2 m $\times$ 0.2 m); (c) and (d) snapshots at 125 ms (c) and 250 ms (d) from SimSonic computations for a source at frequency 20 Hz. One notes the focusing of seismic wave in (d). Alternatively, one might consider applications in ultrasound imaging, with e.g. a source at 2 MHz, and rescale accordingly space and time by a factor 10^5.

controlled release drugs have the advantages of increasing the plasma half-life of therapeutic drugs which are associated with economic benefits such as fewer injections for patients [52] and corresponding reduced healthcare visits.

Upon inspection of figure 11, it can be noted that the house of card type configuration of graphene oxide flakes from transmission electron microscopy (a), which are in the scale of a few micrometers is similar to layers of clay in soils, which are in the scale of a few metres. Following image treatment with Matlab (b), one can export the house of cards geometry in SimSonic and simulate the propagation of a seismic signal upon change of scale by a factor 10^6. The house of cards configuration in figure 10(a) can be exploited to build an effective porous diffusion model for drug diffusion through a graphene oxide membrane as achieved in [3] using mathematical analogies with diffusion models in porous soils, reminiscent of asymptotic techniques used in thin-walled domains, such as acoustic metamaterials [53, 54], if one replaces propagating waves by evanescent pseudo-waves. However, one can see in the present case that upon scaling by a factor one million, and change of the elastic properties for that of clay in soft soil, a seismic lens can be achieved, see figure 11(d). At the nanoscale, one notes that THz pulses excite acoustic phonons [55] and one could thus envisage medical applications in cancer therapy using heat produced by the highly localized phonon field in figure 10(d). One can attribute this elastic field localization to a thin bridge of soft soil (white) between two denser regions of soil (black) at the location of the image, by comparisons of panels (b) and (d). Indeed, it is well known that acoustic and elastic fields oscillate faster in thin domains, see [53, 54] and references therein. We believe that interplay between models and experiments in geophysics and nanoscale biophysics could lead to major discoveries in the near future.

In the present work, we emphasize that in the near future, it would be interesting to identify the possibilities to value the properties of the graphene-sheet structure in civil engineering. Indeed, graphene has a unique band structure with so-called Dirac cones, which are frequencies where the periodic structure behaves like an effective medium with less than ordinary properties, such as a near-zero refractive index allowing for Dirac cone cloaking [56–59]. Thus far, only transmission properties have been studied near Dirac cones, but there may well be also protection features. Let us now move to an outline of what the future of mechanical metamaterials might look like.

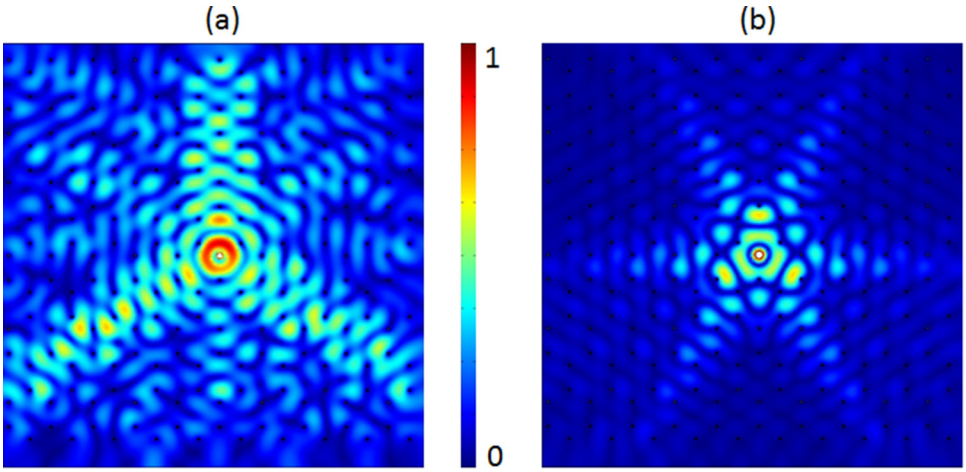

Figure 12. Acoustic source at 100 THz (a) and 110 THz (b) in an atomically thin-plate (0.3 nm) density $\rho = 2.3 \times 10^3$ kg m^{-3}, Young's modulus $E = 10^{12}$ Pa, Poisson ratio $\nu = 0.2$ and flexural plate rigidity $D = 2.34 \times 10^{-18}$ Pa $\times$ m^3 (see [58] for same parameters used in coupling of light and sound in graphene) with clamped inclusions arranged in a honeycomb fashion.

6. Future of mechanical metamaterials across the scales: graphene, bridges and metacities

We have mentioned that acoustic phonons in graphene could have medical applications. Let us now numerically demonstrate an extreme control of an elastic wavefield emitted in a thin plate periodically pinned at vertices of a honeycomb array. We show in figure 12(a) a source oscillating at 100 THz that generates wave pattern with three-fold symmetry, whereas the same source at 110 THz (b) gives rise to six-fold symmetry. Such extreme anisotropy has been unveiled in [57] wherein a mathematical treatment of the Kirchhoff-Love equation led to dynamic effective equations. Here, we apply this result to a graphene sheet treated like an atomically thin plate with parameters as in [58]. Such extreme anisotropy might prove useful in nano-antennae and sensors. A graphene-like pinned plate could also be used to generate highly-directive surface plasmon polaritons when coupling light to it, as proposed in a similar situation in [58].

If we now change scale, and consider soil parameters, we can think of using concrete columns clamped to a bedrock and arranged in a honeycomb fashion to structure soil and create highly directive seismic wave signals. The idea of seismic metamaterials with clamped inclusions has been put forward in [59] and might lead to important applications in civil engineering.

If we now consider 1D periodic structures, low frequency stop bands of inertial resonators like in figure 13(b), which are steel masses connected to a reinforced concrete suspended bridge via steel beams, can disallow propagation of flexural waves along the bridge and thus prevent wobbling of the structures around 3.5 Hz. On the other hand, in panel (a) concrete masses do not match the fundamental mode of the bridge and thus do not prevent its swaying. Indeed, the Millenium bridge was closed down after walk of pedestrians happened to excite one of its fundamental eigenfrequencies [60]. If we assume a time harmonic dependence $\mathrm{e}^{-\mathrm{i}\omega t}$ in (1.3) and (1.4), with ω the angular wave frequency (rad $\cdot$ s^{-1}), a spectral analysis can be performed for so-called Floquet–Bloch waves (ν_1, ν_2) of the form $\nu_j(x_1 + d, x_2) = \nu_j(x_1, x_2)\exp(\mathrm{i}kd)$, $j = 1, 2$ propagating in a bridge which can be considered as a periodic structure with periodicity d along x_1. A closed form representation of the Green's function corresponding to the upper deck of the bridge as in figure 13(a) provides dispersion curves for flexural waves like in panel (c), which are computed here using the commercial finite element package COMSOL Multiphysics. According to [61], the Green's function writes as

$$G(\omega, k) = -\frac{1}{4D\alpha^3}\left(1 + \frac{\cos(kd) - \exp(-\alpha d)}{\cosh(\alpha d) - \cos(kd)} - \frac{\sin(\alpha d)}{\cos(\alpha d) - \cos(kd)}\right) \tag{1.9}$$

where $\alpha = (\rho\omega^2/D)^{1/4}$, with D the normalized flexural rigidity of the beam representing the upper deck of the bridge. We have checked that we retrieve the dispersion curves of figure 3 in [62] for a slender bridge that were computed with the industrial finite element package Strand7 by Dr Giaccu.

The solution proposed in [62] to avoid bridge swaying is a unit cell with two types of masses connected to the upper-deck of the bridge by thin beams and the two-masses are themselves connected by a thin beam. Here, we simply follow the proposal in [63] that was to place underneath the bridge a 1D phononic crystal like in figure 13(e). Unlike for [62], there is a single mass in each unit cell, and an analysis of associated resonant modes reducing unwanted vibrations of the bridge has been performed in [63], notably based on asymptotic estimates of inertial resonators [64, 65]

$$\omega^2 \simeq \frac{\mu\varepsilon^3 h^3}{\pi\rho R^2 l^3}\frac{(\lambda + \mu)}{3(\lambda + 2\mu)} \tag{1.10}$$

where $\lambda = E\nu/[(1+\nu)(1-2\nu)]$ and $\mu = E/[2(1+\nu)]$ are the Lamé constants of reinforced concrete estimated to be 2.8 GPa and 6.6 GPa, respectively, assuming a Young's modulus $E = 2$ GPa and a Poisson's ratio $\nu = 0.33$ in each beam of length $l = 0.4$ m connecting the bridge to the steel resonators. The latter have density $\rho = 7.5 \times 10^3$ kg m^{-3} and their radius is $R = 0.1$ m, with all geometric parameters as in panel (e).

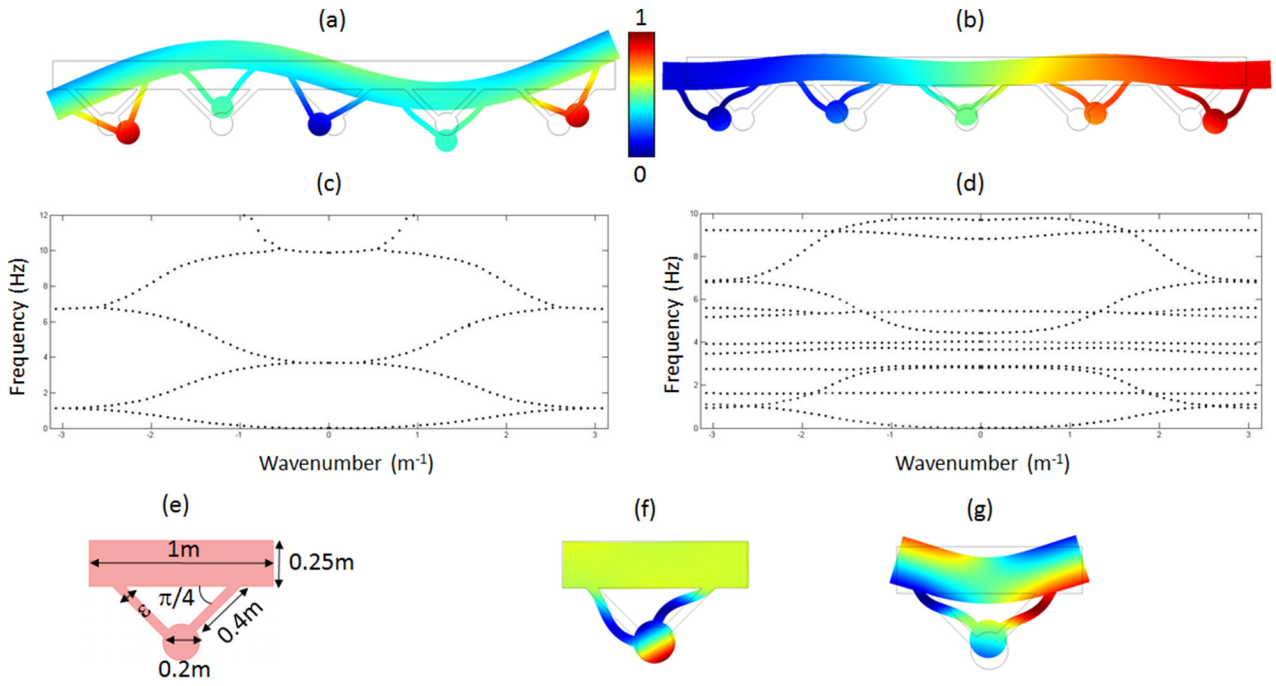

Figure 13. Supercell (10 m) of a periodic array of steel resonators (Young modulus $E = 2 \times 10^{11}$ Pa and density $\rho = 7.5 \times 10^3$ kg m^{-3}) placed underneath a 100 m long beam of reinforced concrete (Young modulus $E = 2 \times 10^{10}$ Pa and density $\rho = 2.5 \times 10^3$kg m^{-3}) simply supported at both ends. The chain of masses connected by steel ligaments to the beam (that consists of 20 supercells, only one is shown) is used as a simplified model for a phononic crystal that suppresses swaying for a bridge that wobbles between 2.9 and 4.5 Hz for a torsional constant of beam section of 2.25 m [4] (i.e. close to the excitation frequency produced in the bridge by a pedestrian walk); (a) unsuppressed vibration of bridge for resonators made of concrete; (b) reduced vibrations of bridge for tuned resonators made of a mass of steel connected to the bridge with concrete ligaments that resonate around 3 Hz; (c) band diagram for the bridge without resonators; (d) band diagram for the bridge with a periodic array of resonators; (e) unit cell used for (d), with $\varepsilon = 0.08$ m small compared to the diameter 0.2 m of the mass; (e) and (f) modes associated with the lower and upper edges of stop band in (d).

We find a resonant frequency $f = \omega/(2\pi) \simeq 3Hz$ for the eigenmode shown in figure 13(f), which corresponds to the second flat band in panel (d), which lies on the lower edge of the phononic band gap.

This design of mechanical metamaterial to avoid bridge swaying could be improved by considering a quasi-periodic chain of resonators, instead of a periodic one, with an expected increase of width and number of low frequency stop bands, and thus a broader frequency range for suppression of unwanted resonances of the bridge. This would make a concept of acoustic rainbow similar to [66]. We note that 3D resonators like in [67] are also good candidates to avoid swaying of the bridge of all sort (lateral, transversal etc).

One could also envisage placing more complex phononic crystals with double or triple periodicity in buildings and other large scale infrastructures to reduce unwanted vibrations caused by traffic noise or earthquakes. For instance, it has been proposed that large scale auxetic metamaterials with dynamically tunable Poisson ratio can make earthquake resistant foundations for buildings in [68].

The proposal in [69] is even more radical as this research group has proposed to use periodic arrays of large scale isochronous resonators as seismic protection. Other types of seismic metamaterials [70, 71] include a large scale version of periodic arrays of inertial resonators inspired by the proposal of Bigoni *et al* [54]. In our opinion, their future will mostly depend upon cost versus seismic protection efficiency.

Finally, one could even consider metamaterials on a larger scale, and think of building meta-cities like in figure 14. This is not a wholly unrealistic idea as the group of Philippe Guéguen in the Institute of Earth Sciences ISTERRE in Grenoble has already put forward the concept of meta-city where buildings play the role of Helmholtz resonators and this bold idea opens a whole new research area in geophysics [72–75].

7. Concluding remarks

In this review article, we have explained how geometric transforms and morphing work and their concepts can be applied to different contexts, such as transformation crystallography, and quasi-crystallography (for which we have recalled the method of cut-and-projection to generated ad libitum quasi-periodic structures). Crystallography is at the base of photonic and phononic crystals, but we stress that it remains valid across scales for large scale seismic metamaterials. Notwithstanding the 1888 theoretical contribution of Lord Rayleigh to crystallography [33], it is widely accepted that this science was boosted over a century ago, by the British physicist, chemist and mathematician Sir William Henry Bragg and his son Sir William Lawrence Bragg. These pioneers in surface science shared the 1915 Nobel Prize in Physics for their discovery of Bragg's law of x-ray diffraction [76], $2d\ \sin\theta = n\lambda$ for constructive interference within an atomic lattice (where d is the atomic spacing in the crystal lattice, n is a positive integer,

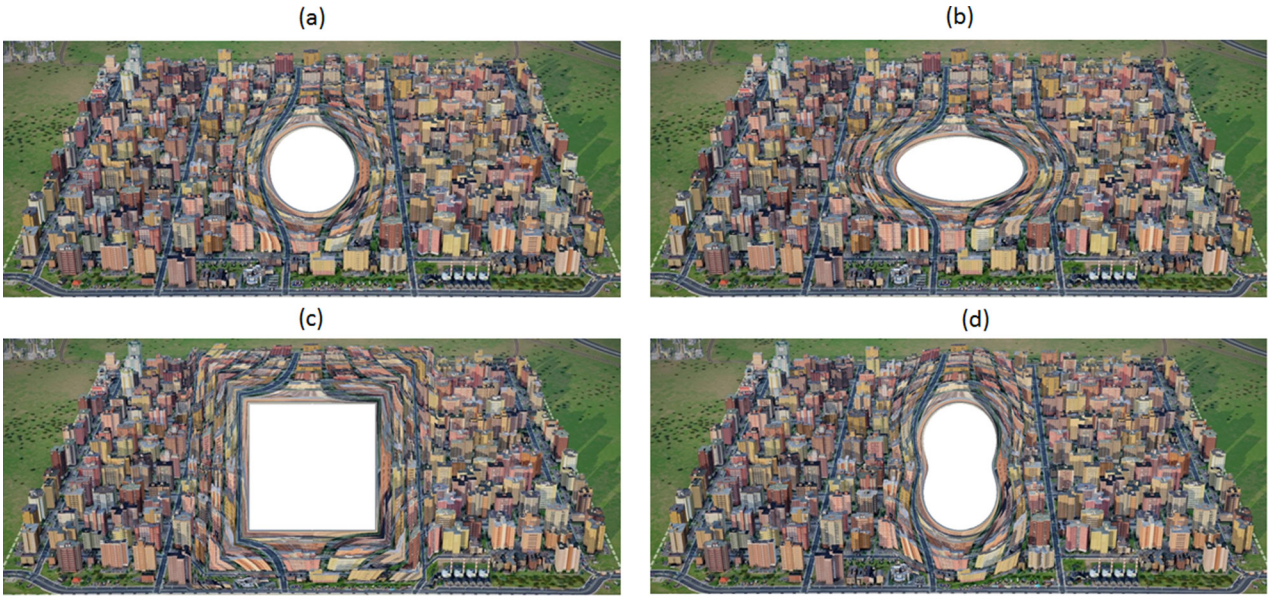

Figure 14. Kilometer scale geometric transforms applied to the schematic representation of a buildup city (a) could be used as a design tool for cities, with an exclusion zone of elliptical (b), square (c) and peanut (d) shapes. This exclusion zone could serve as a safety area for people living in the city in case of earthquakes, and could potentially be landscaped as a park with a lake. Inspired by Martin Wegener's group visionary infography [48].

θ the scattering angle and λ the wavelength of incident wave, which is typically a few angstroms like atomic bonds, so three orders of magnitude shorter than that of light).

Interestingly, Sir William Lawrence Bragg was head of the Cavendish laboratory when the discovery of structure of DNA (deoxyribonucleic acid) was reported by the American biologist James Dewey Watson and his British molecular biologist colleague Francis Crick in 1953. DNA discovery was made possible thanks to scientific discussions with Rosalind Franklin, an English chemist and x-ray crystallographer, who suggested the double helix nature of DNA while working at King's College London.

One can therefore see that crystallography and biology have had a long lasting fruitful joint history, which is certainly due to the similar scales involved (a few nanometers down to angstroms). Graphene, photonic crystals and indeed metamaterials have renewed the interest in crystallography, the former since it (re)opens a door to material science at sub-nanometer scale, the latter since Bragg's scattering is intimately linked to stop bands. However, when viewed from the sky, soils structured at the meter and decameter scale (either through man-made civil engineered techniques or simply arising from in nature, like with forests of trees) display a geometry akin to crystals. We therefore proposed in this article to draw analogies between *seismic metamaterials* and nanoscale crystalline structures to point out the rich history behind the young science of large scale mechanical metamaterials.

We also performed some numerical simulations in elastodynamic wave physics with some mention of applications in mass diffusion, a concept put forward by two of us in [43], which is supported by experiments for an extreme control of heat diffusion process with a thermodynamic cloak, which looks strikingly similar to the mechanical cloak for Lamb waves in plates [39, 77]. A concise graphical summary of the power of morphing is depicted with the comparison of the images in figure 6: The left and right images are almost indistinguishable by the naked eye from a distance i.e. one might think that the corresponding effective media should share many features. However, this is the marked difference between a periodic seismic metamaterial and a transformed seismic metamaterial. The latter wishes to mimic nature's biological structures in order to reproduce some of the (many) interesting features that nature offers. For instance, the famous Morpho butterflies whose wings with an inner grating give their unique structural colors [78, 79]. In the course of this article we have described how morphing can be used to unveil new functionalities by mixing two known transformation-based metamaterials to get a new one which is reminiscent of a complex medium in living cells, which is a form of biomimetism. Morphing may thus prove to be an invaluable tool for the exploration of transformation-based metamaterials from the nanoscale to the metre scale worlds. For instance, as first envisioned in a review paper [80], the group of Martin Wegener proposed to cloak a city, which could be achieved in our case by using the exact same geometric transforms as in figure 1, see figure 14.

The potential research area in seismic metamaterials is vast, looking around for inspiration one notes impressively beautiful quasi-periodic patterns in medieval architecture [81] and we have only touched upon the richness of cloaking phenomenon in the time domain. As stated in [82]: *In the natural world, rays of light are sometimes bent when they pass through air layers of different temperatures, for example one of the most unusual mirages (called the* Fata Morgana *after the fairy Morgana from the Arthurian Legend) bends light rays in such an extreme way that on hot days boats appear to levitate above the sea […] The beauty of Pendry's idea is that it allows matter to be engineered in such a way that light*

follows curved trajectories in metamaterials which are associated with geodesics in a transformed space. In the realm of transformational optics, one can envision many kinds of mirages, simply by distorting the space metric in what amounts to fabricating heterogeneous anisotropic media (also called metamaterials since they have been conceptualized and engineered by mankind). We believe the exciting fields of transformation optics, acoustics, elastodynamics and crystallography are still in their infancy and will lead to unforeseen paradigms. For instance, negative refraction for a flat convergent lens [83] which is a concept arising from optics, has been translated in the area of seismic waves [84]. Amongst new concepts, urban metamaterials [70] may prove a complementary tool to design soundproof and earthquake-resistant civil engineering cloaks in soft soils structured on the metre-scale by columns of concrete. Moreover, it is possible to also control water wave trajectories with similar metamaterial design [85–87]. This was an inspiration for the concept urban city with control of sound waves for reduction of traffic noise [88], as well as seismic metawaveguide put forward in [89]. Last but not least, light, sound and heat interplay might form the essence of soon to come multiphysics small and large-scale metamaterials based on geometric transforms that have proved their utilities for understanding the structure of elements deriving from microscale and very large worlds [90]. The analogies used to translate knowledge gained in one area to another, much smaller or larger, should nonetheless be used wisely, as for instance scalability of phononic crystals breaks down at atomically thin scales [91], so in-depth analysis of elastic waves propagating in graphene such as illustrated in figure 12 requires more advanced models, and models of interactions between soil and structures during earthquakes are highly complex phenomena [92, 93]. We would also like to mention that work on multiscale metamaterials inspired by biomimetism [94] is also emerging with notably fascinating results on spider web-inspired labyrinth acoustic metamaterials [95], that could be further scaled up at the meta-city scale. Transformation-based elastic metamaterials lie somewhere in between these two frontiers (namely the scales of atom and Earth sciences).

Acknowledgments

R Aznavourian, S Guenneau and T M Puvirajesinghe acknowledge the A∗MIDEX project (no ANR-11-IDEX-0001-02) funded by the Investissements d'Avenir French Government program, managed by the French National Research Agency (ANR) with Aix Marseille Université (TMP, A_M-AAP-ID-14-15-140314-09.45-GUENNEAU-PUVIRAJESINGHE-HLS_SAT). S Guenneau also acknowledges European funding through ERC Starting Grant ANAMORPHISM.

ORCID iDs

SébastienGuenneau https://orcid.org/0000-0002-5924-622X

References

[1] Shechtman D, Blech I, Gratias D and Cahn J 1984 Metallic phase with long-range orientational order and no translational symmetry *Phys. Rev. Lett.* **53** 1951–3
[2] Novoselov K S, Geim A K, Morozov S V, Jiang D, Zhang Y, Dubonos S V, Grigorieva I V and Firsov A A 2004 Electric field effect in atomically thin carbon films *Science* **306** 666–9
[3] Puvirajesinghe T M, Zhi Z-L, Craster R V and Guenneau S 2015 Modulation of diffusion rate of therapeutic peptide drugs using graphene oxide membranes *Condens. Matter Mater. Sci.* in preparation (arXiv:1512.08506)
[4] Brûlé S, Javelaud E H, Enoch S and Guenneau S 2014 Experiments on seismic metamaterials: molding surface waves *Phys. Rev. Lett.* **112** 133901
[5] Duneau M and Katz A 1985 Quasiperiodic patterns *Phys. Rev. Lett.* **54** 2688–91
[6] Zolla F, Felbacq D and Guizal B 1998 A remarkable diffractive property of photonic quasi-crystals *Opt. Commun.* **148** 6–10
[7] Della Villa A, Enoch S, Tayeb G, Pierro V, Galdi V and Capolino F 2005 Band gap formation and multiple scattering in photonic quasicrystals with a Penrose-type lattice *Phys. Rev. Lett.* **94** 183903
[8] Guenneau S, Movchan A B, Movchan N V and Trebicki J 2008 Acoustic stop bands in almost-periodic and weakly randomized stratified media: perturbation analysis *Acta Mech. Sin.* **24** 549
[9] Rodriguez A W, McCauley A P, Avniel Y and Johnson S G 2008 Computation and visualization of photonic quasicrystal spectra via Bloch's theorem *Phys. Rev.* B **77** 104201
[10] Lubin S M, Zhou W, Hryn A J, Huntington M D and Odom T W 2012 High-rotational symmetry lattices fabricated by moiré nanolithography *Nano Lett.* **12** 4948–52
[11] Nicolet A, Zolla F and Guenneau S 2008 Finite element analysis of cylindrical invisibility cloaks of elliptical cross section *IEEE Trans. Magn.* **44** 1150–3
[12] Pendry J B, Schurig D and Smith D R 2006 Controlling electromagnetic fields *Science* **312** 1780–2
[13] Zolla F, Guenneau S, Nicolet A and Pendry J B 2007 Electromagnetic analysis of cylindrical invisibility cloaks and mirage effect *Opt. Lett.* **32** 1069
[14] Nicolet A, Zolla F and Guenneau S 2008 Electromagnetic analysis of cylindrical cloaks of an arbitrary cross section *Opt. Lett.* **33** 1584–6
[15] Nicolet A, Remacle J F, Meys B, Genon A and Legros W 1994 Transformation methods in computational electromagnetism *J. Appl. Phys.* **75** 6036–8
[16] Ward A J and Pendry J B 1996 Refraction and geometry in Maxwell's equations *J. Mod. Opt.* **43** 773–93
[17] Vasarely M 2017 www.vasarely.com/
[18] Guenneau F, Chakrabarti S, Guenneau S and Anantha Ramakrishna S 2014 Origami with negative refractive index to generate super-lenses *J. Phys.: Condens. Matter* **26** 405303
[19] Bossy E, Talmant M and Laugier P 2004 Three-dimensional simulations of ultrasonic axial transmission velocity measurement on cortical bone models *J. Acoust. Soc. Am.* **115** 2314–24
[20] Bossy E 2012 www.simsonic.fr/
[21] Diatta A, Kadic M, Wegener M and Guenneau S 2016 Scattering problems in elastodynamics *Phys. Rev.* B **94** 100105
[22] Clouteau D and Aubry D 2001 Modification of the ground motion in dense urban areas *J. Comput. Acoust.* **9** 1659–75

[23] Boutin C and Roussillon P 2006 Wave propagation in presence of oscillators on the free surface *Int. J. Eng. Sci.* **4** 180–204
[24] Terzopoulos D, Platt J, Barr A and Fleischer K 1987 Elastically deformable models *Comput. Graph.* **21** 205–14
[25] Lee S-Y, Chwa K-Y, Hahn J and Shin S Y 1996 Image morphing using deformation techniques *J. Vis. Comput. Animat.* **7** 3–23
[26] Jones J 2017 www.xiberpix.net/SqirlzMorph.html
[27] Aznavourian R and Guenneau S 2014 Morphing for faster computations in transformation optics *Opt. Express* **22** 28301–15
[28] Diatta A and Guenneau S 2016 Elastodynamic cloaking and field enhancement for soft spheres *J. Phys. D: Appl. Phys.* **49** 445101
[29] Diatta A, Achaoui Y, Brûlé S, Enoch S and Guenneau S 2016 Control of Rayleigh-like waves in thick plate Willis metamaterials *AIP Adv.* **6** 121707
[30] Wang Z, Bovik A C, Sheikh H R and Simoncelli E P 2004 Image quality assessment from error visibility to structural similarity *IEEE Trans. Image Process.* **13** 600–61
[31] Yablonovitch E 1987 Inhibited spontaneous emission in solid-state physics *Phys. Rev. Lett.* **58** 2059–62
[32] John S 1987 Strong localization of photons in certain disordered dielectric structures *Phys. Rev. Lett.* **58** 2486–9
[33] Rayleigh J W S 1888 On the remarkable phenomenon of crystalline reflexion described by Prof Stokes *Phil. Mag.* **26** 256–65
[34] Bykov V P 1972 Spontaneous emission in a periodic structure *Sov. J. Exp. Theor. Phys.* **35** 269–73
[35] Ohtaka K 1979 Energy band of photons and low-energy photon diffraction *Phys. Rev.* B **19** 5057–67
[36] Colombi A, Roux P, Guenneau S, Guéguen P and Craster R V 2016 Forests as a natural seismic metamaterial: Rayleigh wave bandgaps induced by local resnances *Sci. Rep.* **6** 19238
[37] Colombi A, Colquitt D, Roux P, Guenneau S and Craster R V 2016 A seismic metamaterial: the resonant metawedge *Sci. Rep.* **6** 27717
[38] Takemiya H and Shimabuku J 2002 Application of soil-cement columns for better seismic design of bridge piles and mitigation of nearby ground vibration due to traffic *J Struct. Eng. Japan Soc. Civil Eng.* **48A** 437–44
[39] Farhat M, Guenneau S and Enoch S 2009 Ultrabroadband elastic cloaking in thin plates *Phys. Rev. Lett.* **103** 024301
[40] Farhat M, Enoch S, Guenneau S and Movchan A B 2008 Broadband cylindrical acoustic cloak for linear surface waves in a fluid *Phys. Rev. Lett.* **101** 1345011
[41] Schittny R, Kadic M, Guenneau S and Wegener M 2013 Experiments on transformation thermodynamics: molding the flow of heat *Phys. Rev. Lett.* **110** 195901
[42] Halimeh J C, Ergin T, Mueller J, Stenger N and Wegener M 2009 Photorealistic images of carpet cloaks *Opt.Express* **17** 19328–36
[43] Guenneau S and Puvirajesinghe T M 2013 Fick's second law transformed: one path to cloaking in mass diffusion *J. R. Soc. Interface* **10** 20130106
[44] Pluen A, Netti P A, Jain R K and Berk D A 1999 Diffusion of macromolecules in agarose gels: comparison of linear and globular configurations *Biophys. J.* **77** 542–52
[45] Magde D, Elson E L and Webb W W 1974 Fluorescence correlation spectroscopy II. An experimental realization *Biopolymers* **13** 29–61
[46] Nair R R, Wu H A, Jayaram P N, Grigorieva I V and Geim A K 2012 Unimpeded permeation of water through helium-leak-tight graphene-based membranes *Science* **335** 442–4
[47] Joshi R K, Carbone P, Wange F C, Kravets V G, Su Y, Grigorieva I V, Wu H A, Geim A K and Nair R R 2014 Precise and ultrafast molecular sieving through graphene oxide membranes *Science* **343** 752–4
[48] Nethravathi C, Viswanath B, Shivakumara C, Mahadevaiah N and Rajamathi M 2008 The production of smectite clay/graphene composites through delamination and co-stacking *Carbon* **46** 1773–81
[49] Zhang R, Alecrim V, Hummelgard M, Andres B, Forsberg S, Andersson M and Olin H 2015 Thermally reduced kaolin-graphene oxide nanocomposites for gas sensing *Sci. Rep.* **5** 7676
[50] Nethravathi C, Rajamathi J T, Ravishankar N, Shivakumara C and Rajamathi M 2008 Graphite oxide-intercalated anionic clay and its decomposition to graphene-inorganic material nanocomposites *Langmuir* **24** 8240–4
[51] Wang J, Liu C, Shuai Y, Cui X and Nie L 2014 Controlled release of anticancer drug using graphene oxide as a drug-binding effector in konjac glucomannan/sodium alginate hydrogels *Colloids Surf.* B **113** 223–9
[52] Ashley G W, Henise J, Reid R and Santi D V 2013 Hydrogel drug delivery system with predictable and tunable drug release and degradation rates *Proc. Natl Acad. Sci. USA* **110** 2318–23
[53] Guenneau S, Movchan A B, Pétursson G and Ramakrishna S A 2007 Acoustic metamaterials for sound focusing and confinement *New J. Phys.* **9** 399
[54] Bigoni D, Guenneau S, Movchan A B and Brun M 2013 Elastic metamaterials with inertial locally resonant structures: application to lensing and localization *Phys. Rev.* B **87** 174303
[55] Maldovan M 2013 Sound and heat revolutions in phononics *Nature* **503** 209–17
[56] Huang X, Lai Y, Hang Z H, Zheng H and Ch S Tan 2011 Dirac cones induced by accidental degeneracy in photonic crystals and zero-refractive-index materials *Nat. Mater.* **10** 582–6
[57] Makwana M, Antonakakis T, Maling B, Guenneau S and Craster R V 2016 Wave mechanics in media pinned at Bravais lattice points *SIAM J. Appl. Math.* **76** 1–26
[58] Farhat M, Guenneau S and Bagci H 2013 Exciting graphene surface plasmon polaritons through light and sound interplay *Phys. Rev. Lett.* **111** 237404
[59] Achaoui Y, Antonakakis T, Brûlé S, Craster R V, Enoch S and Guenneau S 2017 Clamped seismic metamaterials: ultra-low broad frequency stop-bands *New J. Phys.* **19** 063022
[60] Dallard P, Fitzpatrick A J, Flint A, Le Bourva S, Low A, Ridsdill Smith R M and Willford M 2001 The London Millenium Footbridge *Struct. Eng.* **79** 17–33
[61] Brun M, Giaccu G F, Movchan A B and Movchan N V 2012 Asymptotics of eigenfrequencies in the dynamic response of elongated multi-structures *Proc. R. Soc.* A **468** 378–94
[62] Brun M, Movchan A B and Jones I S 2013 Phononic band gap systems in structural mechanics: finite slender elastic structures and infinite periodic waveguides *J. Vibr. Acoust.* **135** 041013
[63] Guenneau S 2010 Modèles multi-échelles pour les métamatériaux électromagnétiques et élastodynamiques *Habilitation à Diriger des Recherches* University of Provence
[64] Guenneau S, Movchan A B and Movchan N V 2007 Localised bending modes in split ring resonators *Physica* B **394** 141–4
[65] Movchan A B, Movchan N V, Guenneau S and McPhedran R C 2007 Asymptotic estimates for localized electromagnetic modes in doubly periodic structures with defects *Proc. R. Soc.* A **463** 1045–67
[66] Zhu J, Chen Y, Zhu X, Garcia-Vidal F J, Yin X, Zhang W and Zhang X 2013 Acoustic rainbow trapping *Sci. Rep.* **3** 1728
[67] Achaoui Y, Ungureanu B, Enoch S, Brûlé S and Guenneau S 2016 Seismic waves damping with arrays of inertial resonators *Extreme Mech. Lett.* **8** 30–7

[68] Ungureanu B, Achaoui Y, Enoch S, Brûlé S and Guenneau S 2015 Seismic auxetic metamaterials as novel earthquake protections *Eur. J. Phys. Appl. Metamater.* **2** 17
[69] Finocchio G, Casablanca O, Ricciardi G, Alibrandi U, Garescì F, Chiappini M and Azzerboni B 2014 Seismic metamaterials based on isochronous mechanical oscillators *Appl. Phys. Lett.* **104** 191903
[70] Krodel S, Thome N and Daraio C 2015 Wide band-gap seismic metastructures *Extreme Mech. Lett.* **4** 111–7
[71] Miniaci M, Krushynska A, Bosia F and Pugno N M 2016 Large scale mechanical metamaterials as seismic shields *New J. Phys.* **18** 083041
[72] Guéguen P, Bard P Y and Chávez-García F J 2002 Site-city seismic interaction in Mexico city-like environments: an analytical study *Bull. Seismol. Soc. Am.* **92** 794–811
[73] Ghergu M and Ionescu I R 2009 Structure-soil-structure coupling in seismic excitation and city effect *Int. J. Eng. Sci.* **47** 342–54
[74] Guéguen P and Colombi A 2016 Experimental and numerical evidence of the clustering effect of structures on their response during an earthquake: a case study of three identical towers in the city of Grenoble, France *Bull. Seismol. Soc. Am.* **106** 2855–64
[75] Brûlé S, Ungureanu B, Achaoui Y, Diatta A, Aznavourian R, Antonakakis T, Craster R V, Enoch S and Guenneau S 2017 *Innov. Infrastruct. Solut.* **2** 20
[76] Bragg W H and Bragg W L 1913 The reflexion of x-rays by crystals *Proc. R. Soc.* A **88** 428–38
[77] Stenger N, Wilhelm M and Wegener M 2012 Experiments on elastic cloaking in plates *Phys. Rev. Lett.* **108** 014301
[78] Vukusic P, Sambles J R, Lawrence C R and Wootton R J 1999 Quantified interference and diffraction in single Morpho butterfly scales *Proc. R. Soc.* B **266** 1402–11
[79] Gralak B, Tayeb G and Enoch S 2001 Morpho butterflies wings color modeled with lamellar grating theory *Opt. Express* **9** 567–78
[80] Kadic M, Bückmann T, Schittny R and Wegener M 2015 Experiments on cloaking in optics, thermodynamics and mechanics *Phil. Trans. R. Soc.* A (https://doi.org/10.1098/rsta.2014.0357)
[81] Lu P J and Steinhardt P J 2007 Decagonal and quasicrystalline Tillings in Medieval Islamic Architecture *Science* **315** 1106–10
[82] Guenneau S 2015 The physics of invisibility *Royal Society* (https://blogs.royalsociety.org/publishing/the-physics-of-invisibility/)
[83] Veselago V G 1968 The electrodynamics of substances with simultaneously negative values of ε and μ *Sov. Phys. Usp.* **10** 509–14
[84] Brûlé S, Enoch S and Guenneau S 2016 Flat lens for seismic waves (arXiv:1602.04492v1)
[85] Berraquero C P, Maurel A, Petitjeans P and Pagneux V 2013 Experimental realization of a water-wave metamaterial shifter *Phys. Rev.* E **88** 051002
[86] Dupont G, Kimmoun O, Molin B, Guenneau S and Enoch S 2015 Numerical and experimental study of an invisibility carpet in a water channel *Phys. Rev.* E **91** 023010
[87] Craster R V and Guenneau S (ed) 2012 *Acoustic Metamaterials* (London: Springer)
[88] Moleron M, Felix S, Pagneux V and Richoux E O 2012 Sound propagation in periodic urban areas *J. Appl. Phys.* **111** 114906
[89] Kim S H and Das M P 2012 Seismic waveguide of metamaterials *Mod. Phys. Lett.* B **26** 1250105
[90] Farhat M, Chen P Y, Guenneau S and Enoch S (ed) 2016 *Transformation Wave Physics: Electromagnetics, Elastodynamics and Thermodynamics* (Singapore: Pan Stanford)
[91] Ramprasad R and Shi N 2005 Scalability of phononic crystals *Appl. Phys. Lett.* **87** 111101
[92] Housner G W 1954 Effect of foundation compliance on earthquake stresses in multistory buildings *Bull. Seismol. Soc. Am.* **44** 551–69
[93] Housner G W 1957 Interaction of building and ground during an earthquake *Bull. Seismol. Soc. Am.* **47** 179–86
[94] Cranford S W, Tarakanova A, Pugno N M and Buehler M J 2017 Nonlinear material behaviour of spider silk yields robust webs *Nature* **482** 72–276
[95] Miniaci M, Krushynska A, Movchan A B, Bosia F and Pugno N M 2016 Spider web-inspired acoustic metamaterials *Appl. Phys. Lett.* **109** 071905